ARL-TR-9025 ● AUG 2020

DEVCOM ARMY RESEARCH LABORATORY

Higher Time-Resolution LASEM, Part III: Influence of Laser-Induced Plasma Chemistry on the Laser-Induced Shock Waves of Aluminized Explosives

by Jennifer L Gottfried

NOTICES

Disclaimers

The findings in this report are not to be construed as an official Department of the Army position unless so designated by other authorized documents.

Citation of manufacturer's or trade names does not constitute an official endorsement or approval of the use thereof.

Destroy this report when it is no longer needed. Do not return it to the originator.

ARL-TR-9025 ● AUG 2020

Higher Time-Resolution LASEM, Part III: Influence of Laser-Induced Plasma Chemistry on the Laser-Induced Shock Waves of Aluminized Explosives

Jennifer L Gottfried
Weapons and Materials Research Directorate, CCDC Army Research Laboratory

REPORT DOCUMENTATION PAGE

Form Approved
OMB No. 0704-0188

1. REPORT DATE *(DD-MM-YYYY)*	2. REPORT TYPE	3. DATES COVERED (From - To)
August 2020	Technical Report	21 November 2019–20 June 2020

4. TITLE AND SUBTITLE
Higher Time-Resolution LASEM, Part III: Influence of Laser-Induced Plasma Chemistry on the Laser-Induced Shock Waves of Aluminized Explosives

5a. CONTRACT NUMBER

5b. GRANT NUMBER

5c. PROGRAM ELEMENT NUMBER

6. AUTHOR(S)
Jennifer L Gottfried

5d. PROJECT NUMBER
622141AH6RK16

5e. TASK NUMBER

5f. WORK UNIT NUMBER

7. PERFORMING ORGANIZATION NAME(S) AND ADDRESS(ES)
CCDC Army Research Laboratory
ATTN: FCDD-RLW-LB
Aberdeen Proving Ground, MD 21005-5069

8. PERFORMING ORGANIZATION REPORT NUMBER
ARL-TR-9025

9. SPONSORING/MONITORING AGENCY NAME(S) AND ADDRESS(ES)

10. SPONSOR/MONITOR'S ACRONYM(S)

11. SPONSOR/MONITOR'S REPORT NUMBER(S)

12. DISTRIBUTION/AVAILABILITY STATEMENT
Approved for public release; distribution is unlimited.

13. SUPPLEMENTARY NOTES
ORCID ID: Jennifer Gottfried, 0000-0002-1282-1928

14. ABSTRACT
In this final installment of our report series on higher time-resolution data from an improved laser-induced air shock from energetic materials (LASEM) setup, we compare the energy release and spectroscopic emission following pulsed laser excitation of trinitrotoluene (TNT) and hexanitrohexaazaisowurtzitane (CL-20) with either 19% or 10% by weight aluminum nanoparticles (nano-Al). The addition of nano-Al significantly reduces the characteristic laser-induced shock velocities (i.e., estimated detonation velocities), the chemical energy behind the shock wave, and the temperature of the surrounding air. However, the plasma temperatures and electron densities calculated using the hydrogen emission lines were higher for the aluminized explosives. Clear differences in the plasma and combustion chemistry were observed for aluminized TNT and CL-20 via ultraviolet, visible, and near-infrared emission spectroscopy, illustrating the effect of oxygen balance on the Al oxidation during different stages of the energy release (<10 μs, 10s of μs, and 10s of ms).

15. SUBJECT TERMS
laser-induced air shock from energetic materials, LASEM, laser-induced shock wave, emission spectroscopy, detonation performance, aluminum

16. SECURITY CLASSIFICATION OF:			17. LIMITATION OF ABSTRACT	18. NUMBER OF PAGES	19a. NAME OF RESPONSIBLE PERSON
a. REPORT	b. ABSTRACT	c. THIS PAGE			Jennifer L Gottfried
Unclassified	Unclassified	Unclassified	UU	48	19b. TELEPHONE NUMBER (Include area code) (410) 278-7573

Standard Form 298 (Rev. 8/98)
Prescribed by ANSI Std. Z39.18

Contents

List of Figures

List of Tables

Acknowledgments

The author wishes to thank Dr Brian Barnes for developing an edge-detection algorithm to measure the laser-induced shock wave positions and providing results used in this report. This project was primarily funded by the US Army Combat Capabilities Development Command (CCDC) Army Research Laboratory's (ARL's) 6.2 Energetics Mission Program in support of the CCDC Army Research Laboratory's Long-Range Distributed and Collaborative Engagements essential research area and the Army's top modernization priority Long-Range Precision Fires. Funding for new diagnostic equipment was provided by the US Department of Defense, Office of the Under Secretary for Defense for Research and Engineering, Applied Research for the Advancement of Science and Technology Priorities Program on Enhanced Energetic Effects under Task 2: Accelerating MAGIC (Materials Adding Gurney through Inorganic Chemistry).

1. Introduction

In Part I of this report series,[1] we presented data on aluminum (Al) materials (a bulk Al alloy plate, micrometer-sized powder [micron-Al], nanoparticles [nano-Al]) acquired with an upgraded laser-induced air shock from energetic materials (LASEM) setup. In that work, we confirmed that nano-Al releases more energy on the microsecond timescale than micron-Al. This result was also supported by the more intense, earlier emission from the oxidation intermediate aluminum monoxide (AlO) by nano-Al on the microsecond timescale compared to either micron-Al or bulk Al. At longer timescales during the combustion of Al at lower temperatures, the time to peak AlO emission followed the expected trends in ignition temperatures, that is, nano-Al < micron-Al.

Subsequently, in Part II we investigated the influence of plasma chemistry on the laser-induced shock waves and spectroscopic signatures of five common military explosives: trinitrotoluene (TNT), triaminotrinitrobenzene (TATB), cyclotrimethylene trinitramine (RDX), cyclotetramethylene tetranitramine (HMX), and hexanitrohexaazaisowurtzitane (CL-20).[2] The higher time-resolution LASEM data acquired at 420,000 frames per second (fps) rather than the original 84,000 fps[3] was used to demonstrate that the timescale for chemical reactions of the ablated material to influence the plasma chemistry and resulting shock wave is between approximately 1–8 μs. In addition, a new calibration curve was developed to correlate the laser-induced shock waves to the measured detonation velocities from large-scale testing, resulting in a higher R^2 value for the linear fit (R^2 = 0.9994 vs. 0.9939) and similar confidence intervals using the data from only 20 laser shots per sample versus 40+ laser shots per sample for the original calibration. The effect of the high-temperature explosive chemistry on the near-infrared (NIR) emission features was also explored for the first time.

Because of its high oxidation enthalpy (31 kJ/g) and widespread availability, Al is of interest as a fuel source for a wide range of energetic applications including thermites, pyrotechnics, propellants, and explosives.[4–9] The mechanisms for oxidation of Al have been an active area of investigation for many years.[10–12] The addition of Al to energetic materials with or without external oxidizers significantly complicates the reaction chemistry. It has also been demonstrated that the reaction mechanisms for metal composites depend on the heating rate[13]; unlike other nondetonative techniques used to study these materials, the heating rates for LASEM are comparable to those during a detonation (~10^{13} K/s).

In addition to studying the influence of Al on the laser-induced plasma chemistry of RDX,[14] we previously used the original LASEM setup to investigate the energy

release from aluminized explosives. Mixtures of RDX, TNT, 3,4-bis(4-nitro-1,2, 5-oxadiazol-3-yl)-1,2, 5-oxadiazole-*N*-oxide (DNTF, also known as BNFF), and 3,4-bis(4-nitro-1,2,5-oxadiazol-3-yl)-1,2,5-oxadiazole (LLM-172, also known as BNFF-1) with commercial micron-Al additives have been studied by our group.[15] TNT mixtures with novel core-shell nano-Al particles encased in an iodate-based oxidizer,[16,17] with graphene-oxide-wrapped micron-Al or nano-Al particles,[18,19] or with ball-milled Al:zirconium (Zr) composites[20] have also been investigated with the original LASEM setup.

Nanoscale Al has a lower ignition temperature and is expected to react faster in energetic material formulations. Here, we investigate mixtures of an oxygen-poor explosive TNT or a powerful, more oxygen-balanced explosive CL-20 with a commercial nano-Al powder using the upgraded LASEM setup. The properties of this specific nano-Al have been investigated with the current setup in Part I,[1] and with many additional techniques in a recent comparison of commercial Al powders.[21]

2. Experimental

2.1 Sample Preparation

The TNT and CL-20 were obtained from colleagues at the US Army Combat Capabilities Development Command (CCDC) Army Research Laboratory (ARL). An "Al nanopowder" sample from Sigma-Aldrich with a mean nanoparticle size of 110 ±2 nm (determined via dynamic light scattering)[21] was used as an explosive additive. This sample also contains larger, micron-sized Al particles as well (as observed via scanning electron microscopy and thermogravimetric analysis).[21] Based on the optimum Al concentration determined from large-scale detonation testing or thermochemical analysis using micron-Al, mixtures of approximately 20% nano-Al with TNT[4] and 10% nano-Al with CL-20[22,23] by mass were prepared by weighing each of the components into a vial. The samples were then physically mixed with a spatula until the dark Al powder appeared homogeneously distributed throughout the lighter-colored explosive. Next, the samples were prepared as previously described for other LASEM experiments.[3,24] Each explosive was spread onto double-sided tape affixed to a 75- × 25-mm glass microscope slide (Fig. 1).

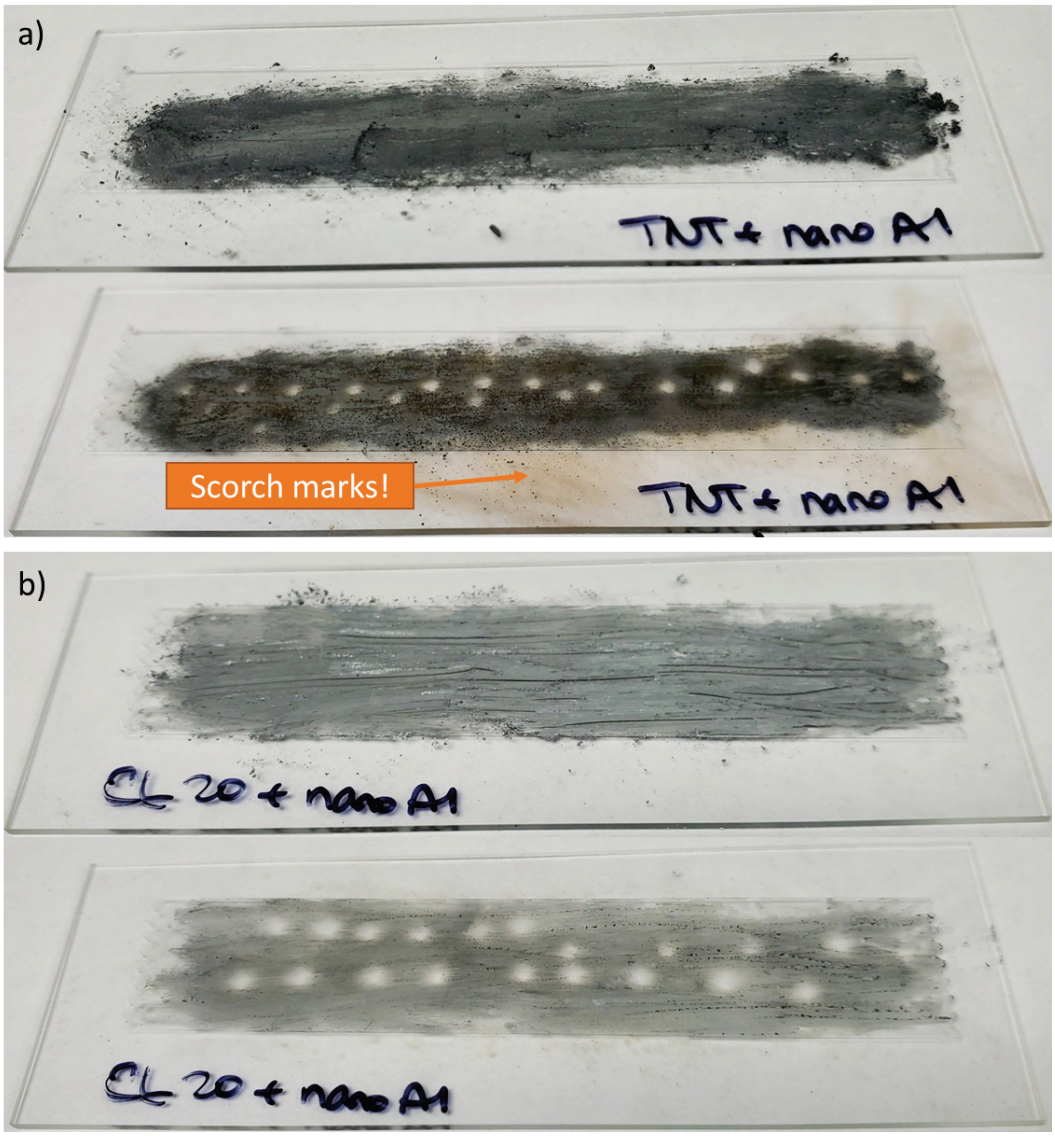

Fig. 1 Prepared sample slides including a) TNT + 19% Al and b) CL-20 + 10% Al. The first slide in each series consists of the as-prepared slide; subsequent images in each series show the slide after 20 laser shots.

Table 1 lists the wt% Al in each mixture, the amount of mixed material added to each slide, and the approximate surface coverage prior to data collection. Twenty laser shots were acquired for each sample.

Table 1 Sample slide surface coverage for the aluminized explosive materials

Sample	Al wt%	Material mass (mg)	Est. slide coverage (mg/cm^2)
TNT + Al	19.2	11.8	1.62
CL-20 + Al	10.1	7.70	0.906

2.2 LASEM Configuration

The experimental setup used to collect the sample data was described in Part I of this report series.[1] Following pulsed laser excitation of the prepared samples (20 laser shots each), various diagnostic data were collected for each sample to understand the influence of the high-temperature chemistry on the laser-induced plasma properties and the resulting material reactions. Table 2 summarizes the diagnostic methods and instrument settings used for this work.

Table 2 Experimental diagnostics, measured data, and instrument settings for the current study

Diagnostic method	Data collected	Instrument settings
High-speed schlieren imaging	Laser-induced shock wave propagation into air above sample	420,000 fps; 369-ns shutter; image size 832 × 16 pixels
High-resolution gated plasma emission spectroscopy	Laser-induced plasma emission in the 200–1000-nm range (0.02-nm resolution)	1.5-µs delay, 10-µs gate width; intensified charge-coupled detector (ICCD) gain = 900
Time-resolved emission detection with two monochromator/ photomultiplier tubes (PMTs)	Emission at 486.58 ±0.02 nm and 656.100 ±0.004 nm	Relative intensities calibrated with a tungsten-halogen light source; PMT gains = 1 for the neat explosives and nano-Al; PMT gains = 3 for the aluminized explosives
Combustion emission spectroscopy	Combustion emission in the 230–900-nm range (0.25-nm resolution)	200-µs delay, 4-ms gate width
Sequential emission spectroscopy	100 sequential spectra obtained using two linked spectrometers, from 200 to 1100 nm (1.4-nm resolution) and from 1000 to 2500 nm (8.9-nm resolution)	1.5-µs delay, 1.050-ms gate width from 200 to 1100 nm and 500-µs gate width from 1000 to 2500 nm
Time-resolved infrared (IR) emission detection	Integrated IR emission (900–1700 nm)	Gain = 3×10^3 (CL-20); gain = 3×10^2 (TNT, TNT + nano-Al, CL-20 + nano-Al); gain = 3 × 10 (nano-Al)

3. Results

3.1 High-Speed Imaging of Laser-Induced Shock Waves

Figure 2 shows snapshots from the typical schlieren video for nano-Al, TNT, CL-20, TNT + nano-Al, and CL-20 + nano-Al. Strong continuum, atomic, and ionic emission from Al results in saturation of the high-speed camera in the first frame, while the pure energetic materials have significantly less emission as discussed in Part II.[2] The color camera shows blue emission from the excited AlO intermediate species continuing beyond 25 μs and is also present at 155 μs for both nano-Al and the CL-20 + nano-Al mixture. The purple emission is due to cyano radical (CN) emission from recombination reactions following laser ablation of the energetic materials.

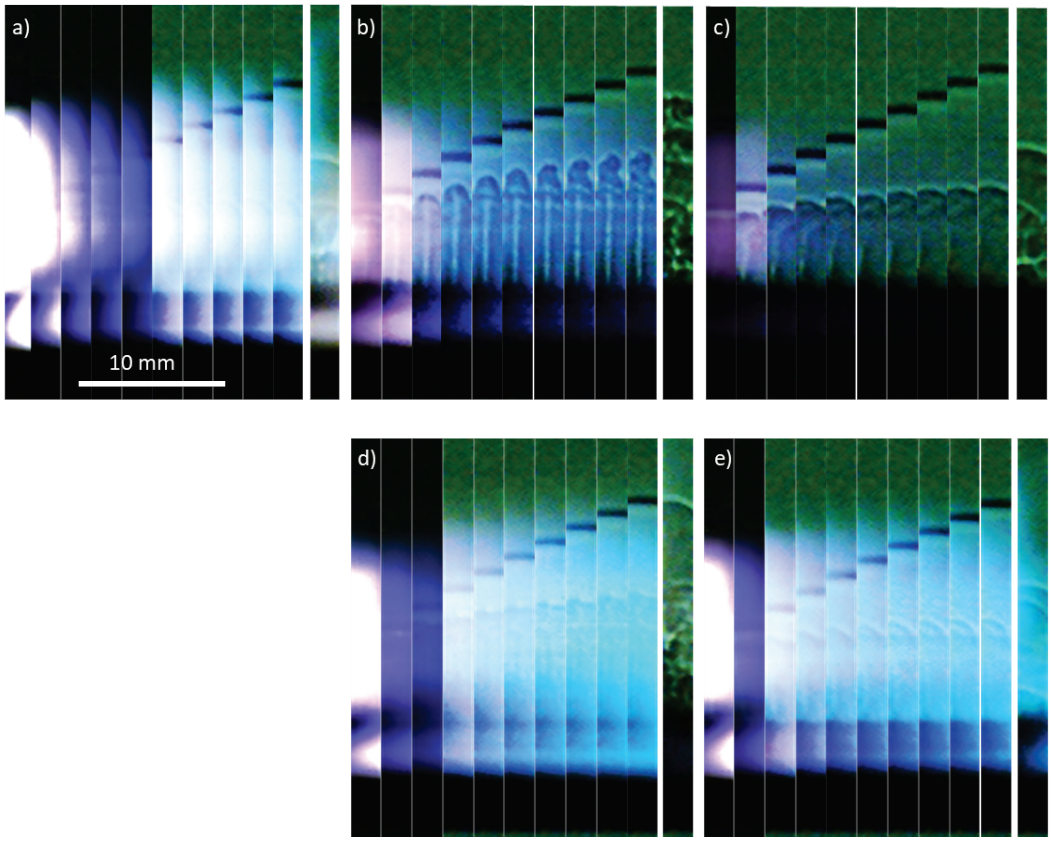

Fig. 2 Snapshots from the high-speed video acquired following laser excitation of a) nano-Al powder, b) TNT, c) CL-20, d) TNT + nano-Al, and e) CL-20 + nano-Al. The first 10 frames cover the time from 0 to 23.8 μs and the last frame of each series is from 155 μs. All images have been cropped from the top, and later frames of each series were adjusted for brightness (+70%) and contrast (+20%) to enhance visualization of the laser-induced shock wave, as indicated by the green background. White emission is due to continuum plasma emission, purple indicates CN emission, and blue indicates AlO emission.

3.2 Measurements of Laser-Induced Shock Wave Positions

As discussed in Part II,[2] the laser-induced shock wave positions were manually measured for the early frames and an automated edge-detection algorithm was used to measure the shock wave position once the shock wave exited the plasma region. Since the addition of nano-Al increased the plasma emission intensity and duration (Fig. 2), the shock position in more frames had to be manually measured than for the pure energetic materials. For example, with TNT the shock wave position was partially obscured for 3–6 frames, while for TNT + nano-Al the shock wave position had to be manually measured for 6–7 frames. Figure 3 compares the laser-induced shock wave positions for TNT versus TNT + nano-Al and CL-20 versus CL-20 + nano-Al for the first 10 μs. While the average shock wave position was higher in the first frame for TNT + nano-Al than TNT, the shock wave position for TNT was higher for subsequent frames. After approximately 20 μs, the shock wave positions became indistinguishable (Fig. 4). Since the laser-induced shock wave has already passed through the plasma region by this point, changes in the temperature of the surrounding air that influence the speed of sound in air (as shown in Part II)[2] may be responsible for the observed differences at later times. The shock wave positions for the CL-20 and CL-20 + nano-Al were indistinguishable in the first, third, and fourth frames—but higher for CL-20 in the second and fifth frames. After approximately 20 μs, the CL-20 shock position was slightly higher than for CL-20 + nano-Al (Fig. 4). This suggests the kinetics of the plasma chemistry may be more complex for the CL-20 mixture—but the relatively large confidence intervals necessitate caution drawing conclusions without confirmatory experiments.

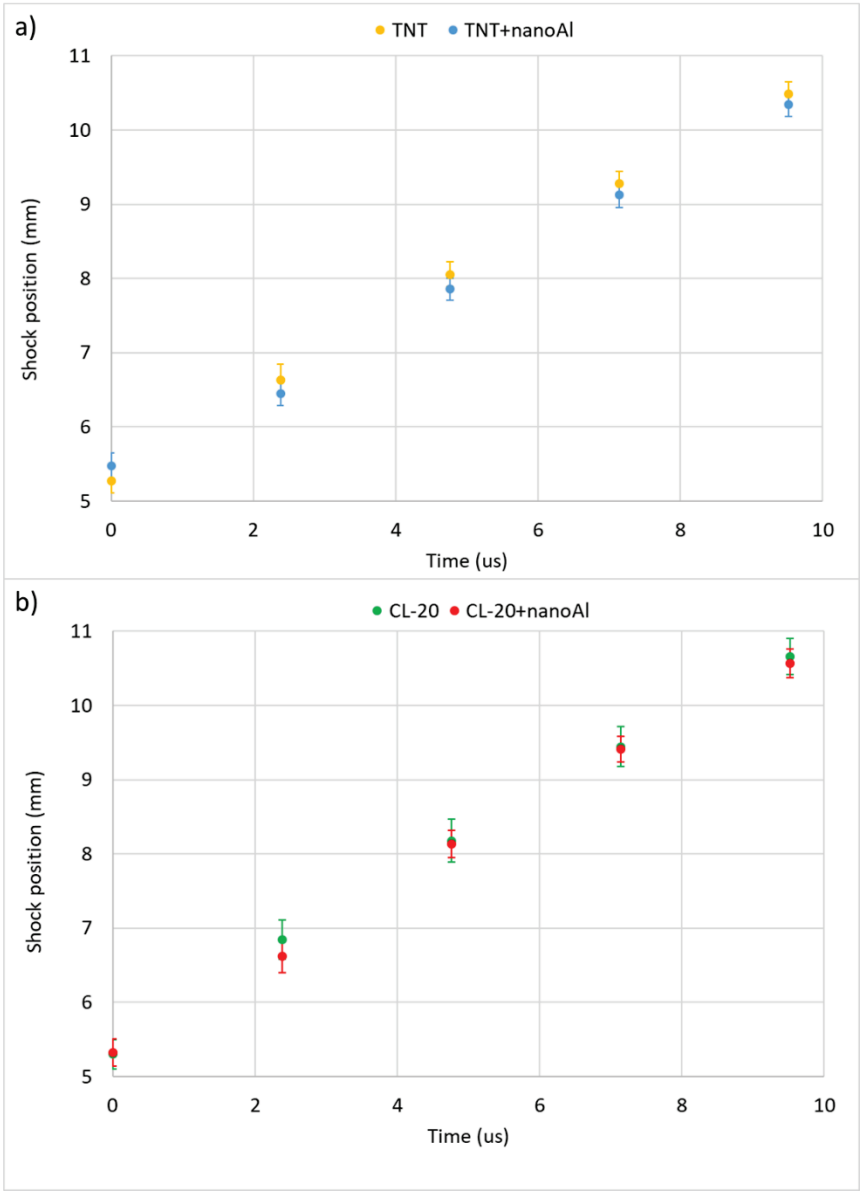

Fig. 3 Average laser-induced shock wave position above the sample surface as a function of time for a) TNT vs. TNT + nano-Al and b) CL-20 vs. CL-20 + nano-Al during the first 10 µs. Error bars are 95% confidence intervals.

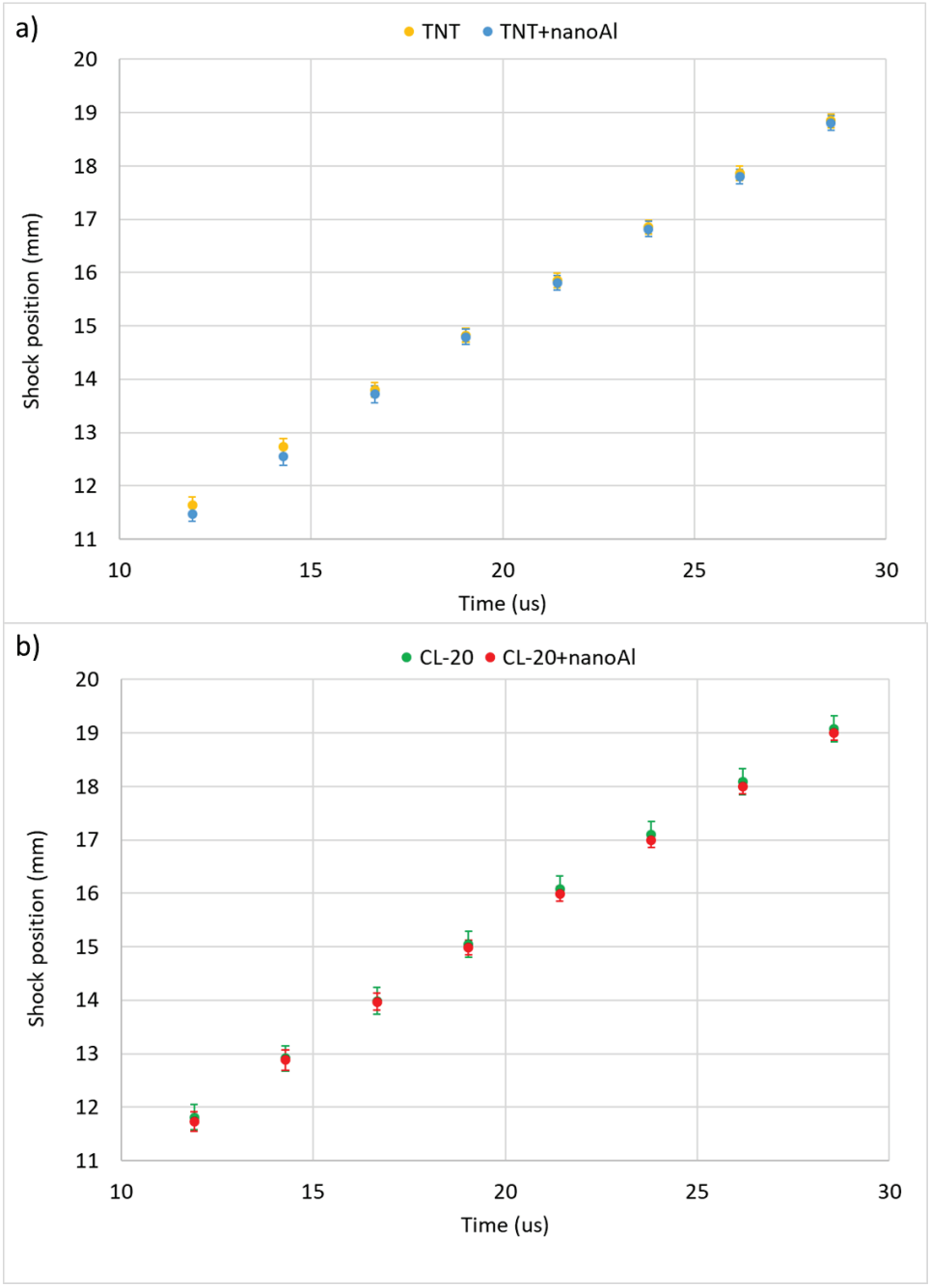

Fig. 4 Average laser-induced shock wave position above the sample surface as a function of time for a) TNT vs. TNT + nano-Al and b) CL-20 vs. CL-20 + nano-Al from 10 to 30 µs. Error bars are 95% confidence intervals.

3.3 Characteristic Laser-Induced Shock Wave Velocities

The laser-induced shock velocities as a function of time were measured using the "backwards difference" method and fit to a fifth-order polynomial, as described in Part II.[2] Figure 5 shows the average laser-induced shock velocities for TNT,

TNT + nano-Al, CL-20, and CL-20 + nano-Al. For both TNT and CL-20 (Table 3), the addition of nano-Al significantly reduced the characteristic laser-induced shock velocity (y-intercept of the polynomial fit); this decrease was –8.8% for TNT (19% nano-Al) and –8.6% for CL-20 (10% nano-Al). Table 3 also includes the estimated detonation velocity for each explosive material based on the correlation determined in Part II, Fig. 13.[2] The addition of nano-Al reduces the estimated detonation velocities for both explosives, as previously observed for large-scale detonation testing.[25,26] Because more nano-Al reacts on the microsecond timescale, scavenging oxygen from the explosive, this effect is more pronounced than that observed with micron-Al.[14,15,25] However, other reports suggest that nano-Al could increase the performance of explosives under certain conditions (compared to the pure explosive,[27] the explosive plus an inert additive,[4,26,28,29] or the explosive with micron-Al additive[23,27,30–35]).

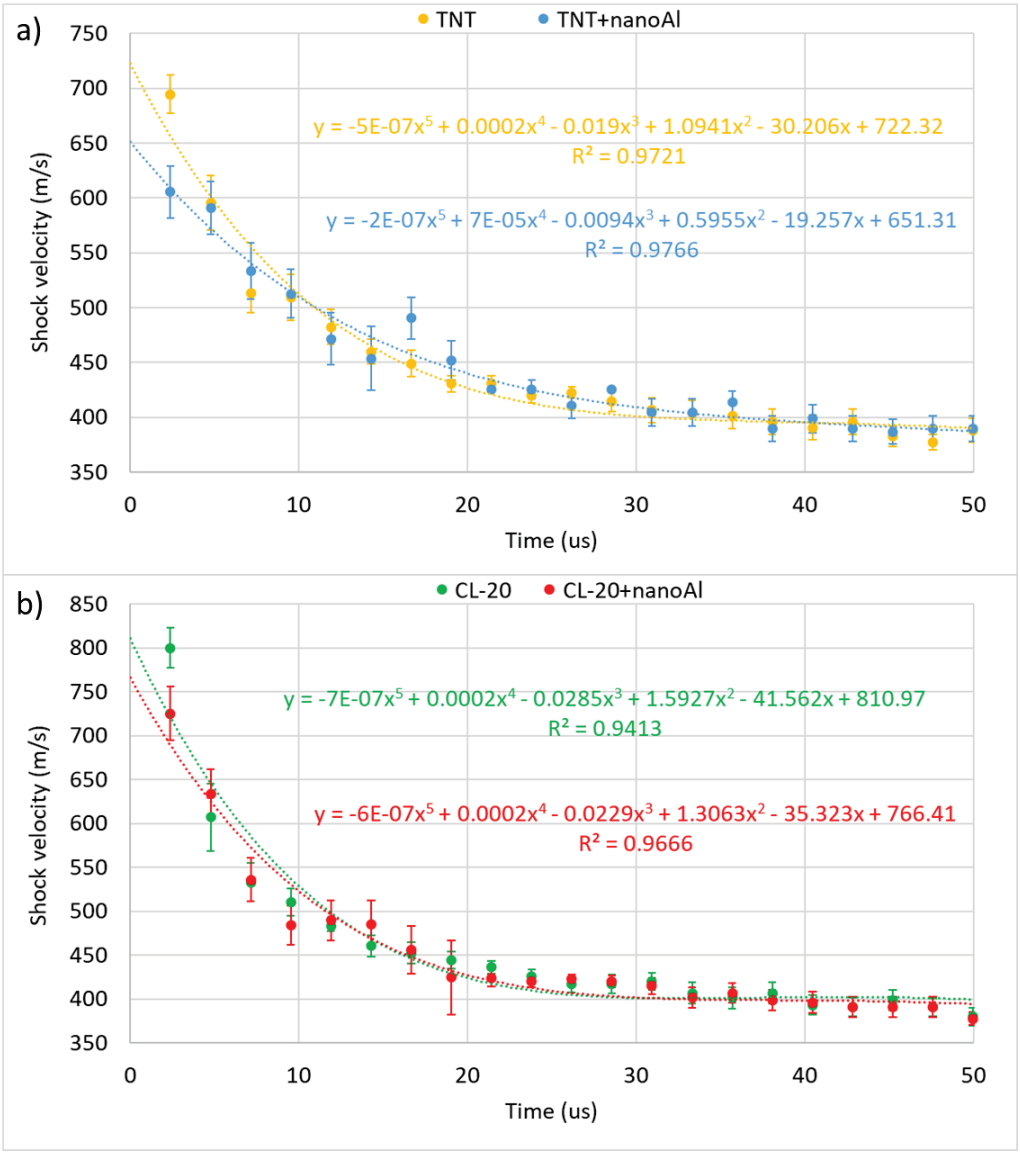

Fig. 5 Average laser-induced shock velocities as a function of time for a) TNT vs. TNT + nano-Al and b) CL-20 vs. CL-20 + nano-Al with fifth-order polynomial fits. Error bars are 95% confidence intervals. The y-intercept is the characteristic laser-induced shock velocity for the sample.

Table 3 Characteristic laser-induced shock velocities and estimated detonation velocities for nano-Al, TNT, TNT + nano-Al, CL-20, and CL-20 + nano-Al

Sample [Ref]	Average characteristic laser-induced shock wave velocity (m/s)	Estimated detonation velocity @ TMD (km/s)
nano-Al [1]	787.71 ±8.19	N/A
TNT [2]	722.32 ±9.29	7.02 ±0.27
TNT + nano-Al	651.31 ±9.91	5.19 ±0.29
CL-20 [2]	810.97 ±7.34	9.56 ±0.21
CL-20 + nano-Al	766.41 ±8.90	7.55 ±0.26

CHEETAH[36] calculations for TNT and CL-20 with and without Al (19% and 10% by weight, respectively) were performed. The correlation between the estimated detonation velocities of the pure explosives and their calculated detonation velocities is strong ($R^2 = 0.9543$) (Fig. 6), although not as strong as the correlation with measured detonation velocities ($R^2 = 0.9994$: Part II, Fig. 13).[2] Although CHEETAH does not incorporate morphology effects into the thermochemical code, the Al can be designated as active (i.e., participates in the detonation chemistry) or inactive. Due to the high laser-induced shock velocities for the pure nano-Al sample, which indicated it is more reactive on the microsecond timescale than micron-Al, 100% of the nano-Al was assumed to be active for the purposes of the CHEETAH calculations. As shown in Fig. 6, the estimated detonation velocities are even lower than expected based on the calculated values. Assuming any fraction of the nano-Al is inert increases the calculated detonation velocities.

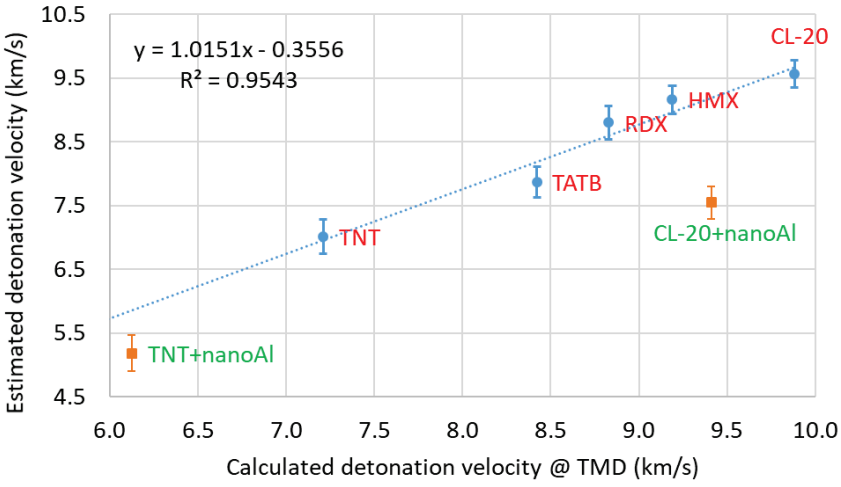

Fig. 6 Correlation between estimated detonation velocities from LASEM and calculated detonation velocities from CHEETAH[36]

While no direct comparison of the higher time-resolution LASEM data for the aluminized explosives to data acquired with the original LASEM setup is available,

Fig. 7 compares the characteristic laser-induced shock wave velocities for TNT, TNT + micron-Al, and TNT + nano-Al (~20 wt% Al) acquired with either the original LASEM setup or the current, higher time-resolution setup. Although the laser-induced shock velocities are slightly lower for pure TNT with the new LASEM setup, the drop in laser-induced shock velocities for TNT + nano-Al (i.e., estimated detonation velocities) is even more significant with the current LASEM setup. The difference is that two different nano-Al samples were used—a highly agglomerated nano-Al sample from NovaCentrix was used for the original LASEM setup, while a Sigma-Aldrich sample with a slightly larger particle size (but significantly less agglomeration) was used for the current study. The NovaCentrix sample was previously found to behave similarly to micron-Al on the microsecond timescale due to the agglomeration, while the nano-Al used in the current study provided the strongest laser-induced shock velocity among the nine different commercial Al samples studied.[21] This suggests that the Sigma-Aldrich "nano" Al sample is more reactive than the 80-nm NovaCentrix Al on the microsecond timescale. As a result, the "nano" Al sample may scavenge more oxygen from the TNT mixture during the detonation-relevant time regime—thus further reducing the estimated detonation velocity.

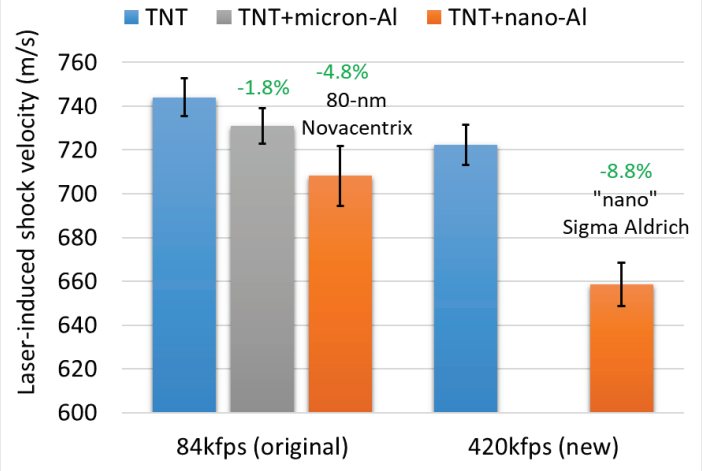

Fig. 7 Comparison of characteristic laser-induced shock velocities for aluminized TNT acquired with either the original LASEM setup at 84,000 fps or the current setup at 420,000 fps

Factors that affect the rate and extent of Al oxidation include the properties of the Al particles: particle size/shape, oxide layer phase/porosity/thickness, impurities, agglomeration, surface functional groups, proximity to oxidizer, and proximity to early exothermic reactions (e.g., alternative shell compositions). In addition, formulation properties influence the Al oxidation: ratio of Al/explosive, porosity/density, oxygen balance, chemistry of the reacting explosive (detonation products, temperature, etc.), and other ingredients in the formulation (energetic or

inert binders, plasticizers, etc.). Finally, the experimental conditions such as charge diameter and degree of confinement during the detonation event influence the Al oxidation. Such conditions cannot be replicated with LASEM experiments; however, the lab-scale experiments can be used to help optimize the chemistry to increase the rate and extent of Al oxidation in the explosive formulation. Ultimately, for increased detonation performance the Al should react on the microsecond timescale to influence detonation velocity or Gurney energy, and for increased blast or fireball the Al should react on the millisecond (or longer) timescale. Achieving an increase in detonation velocity or Gurney energy with the addition of Al will require the use of novel Al additives and/or precise optimization of the energetic formulation.

3.4 Other Measurements of Energy Release

As described in detail in Part II,[2] a double exponential fit with an offset can be fit to the laser-induced shock velocity versus time to determine the speed of sound in air y_0—and thus, the temperature of the surrounding air (Table 4). These results confirm the characteristic laser-induced shock velocity results, which demonstrated a decrease in energy release on the microsecond timescale with the addition of nano-Al. The addition of nano-Al to either TNT or CL-20 decreased the amount of energy transferred to the surrounding air, resulting in lower air temperatures following the laser-induced chemical reactions of aluminized explosives.

Table 4 Experimentally determined speed of sound in air, calculated air temperature, and double exponential fit coefficients

Sample [Ref]	y_0 (m/s)	Calc. T_{air} °C (°F)	A_1	τ_1 (µs)	A_2	τ_2 (µs)
TNT [2]	361.2 ±2.3	49.5 (121)	185.0 ±13.2	3.5 ±0.4	148.6 ±11.5	25.0 ±2.6
CL-20 [2]	366.6 ±1.5	58.5 (137)	268.6 ±8.4	2.3 ±0.1	164.1 ±6.8	22.8 ±1.4
TNT + nano-Al	353.2 ±18.1	36.2 (97.1)	175.6 ±57.8	9.7 ±2.9	85.3 ±44.2	46.5 ±45.6
CL-20 + nano-Al	359.1 ±4.4	46.0 (114.8)	240.6 ±18.3	4.2 ±0.5	130.2 ±15.1	30.6 ±5.8

Another measurement of the energy release behind the shock wave uses the Sedov-Taylor model described in Part II[2] to fit the experimental data. Table 5 shows the fit coefficients from a combination Sedov-Taylor and drag model fit, along with the calculated energy behind the shock wave (based on the A coefficient and Eq. 5 in Part II).[2] The calculated chemical energy behind the shock wave for the pure explosives was previously shown to be strongly correlated to measured detonation velocities ($R^2 = 0.9920$); for comparison, the calculated energies for aluminized

explosives are shown in Fig. 8. While the TNT + nano-Al data point fits the linear correlation determined by the pure explosives, CL-20 + nano-Al is an outlier—suggesting that the actual detonation velocity may be lower than that predicted by CHEETAH. This agrees with the lower estimated detonation velocity from LASEM based on the y-intercept of a fifth-order polynomial fit of the laser-induced shock wave velocities (Fig. 6).

Table 5 Fit coefficients, χ^2 value for the goodness of fit, and calculated energy behind the laser-induced shock wave

Sample [Ref]	*A*	R_0	β	χ^2	*E* (mJ)
TNT [2]	0.411 ±0.009	5582 ±1e7	0.06 ±113	1877	12.8 ±1.3
CL-20 [2]	0.485 ±0.009	5524 ±1e7	0.06 ±114	2100	29.1 ±2.7
TNT + nano-Al	0.357 ±0.026	5532 ±3e7	0.06 ±329	12,294	2.92 ±2.30
CL-20 + nano-Al	0.448 ±0.010	5407 ±1e7	0.06 ±122	3423	16.2 ±2.19

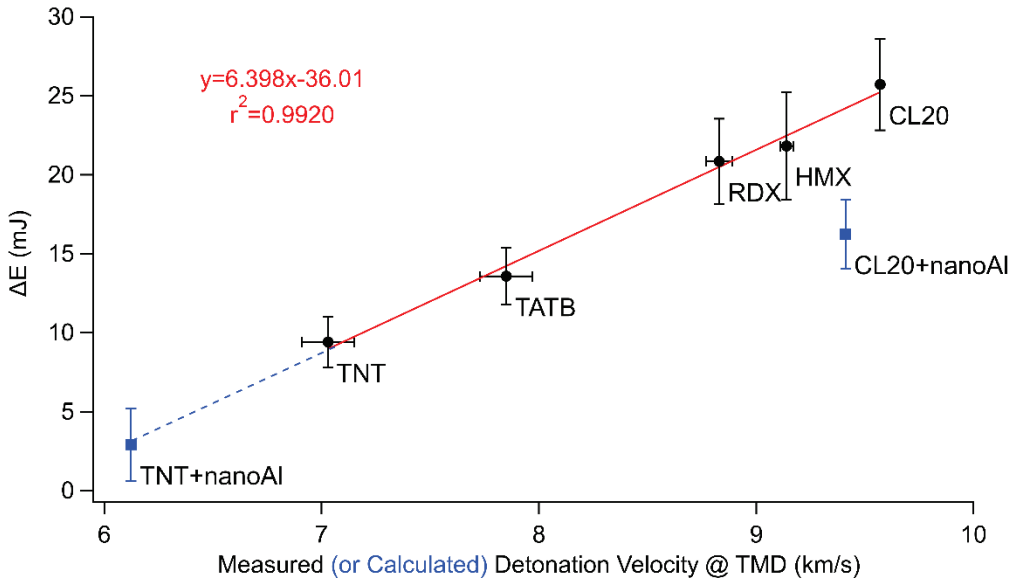

Fig. 8 Correlation between calculated chemical energy and measured detonation velocities from the pure explosives. Calculated detonation velocities from CHEETAH[36] were used for the aluminized explosives.

3.5 High-Resolution Plasma Emission Spectroscopy

3.5.1 Spectral Intensities and Ratios

The average laser-induced emission spectra (integrated from 1.5 to 11.5 μs after the laser pulse) for the nano-Al, TNT, and CL-20 mixtures are shown in Fig. 9. Prominent emission features include atomic and ionic emission due to metal components such as Al, magnesium (Mg), copper (Cu), iron (Fe), and zinc (Zn); organic components such as carbon (C), hydrogen (H), nitrogen (N), and oxygen (O); and common alkali/alkaline earth impurities sodium (Na), potassium (K), and lithium (Li). Molecular species formed through recombination reactions as the plasma cools include diatomic carbon (C_2), CN, and AlO. The nano-Al sample contains many metallic and organic impurities, while the neat TNT and CL-20 consist primarily of CHNO-related species. These emission features can be used to compare the relative intensities of various species as a function of plasma chemistry and to calculate plasma temperatures and electron densities.

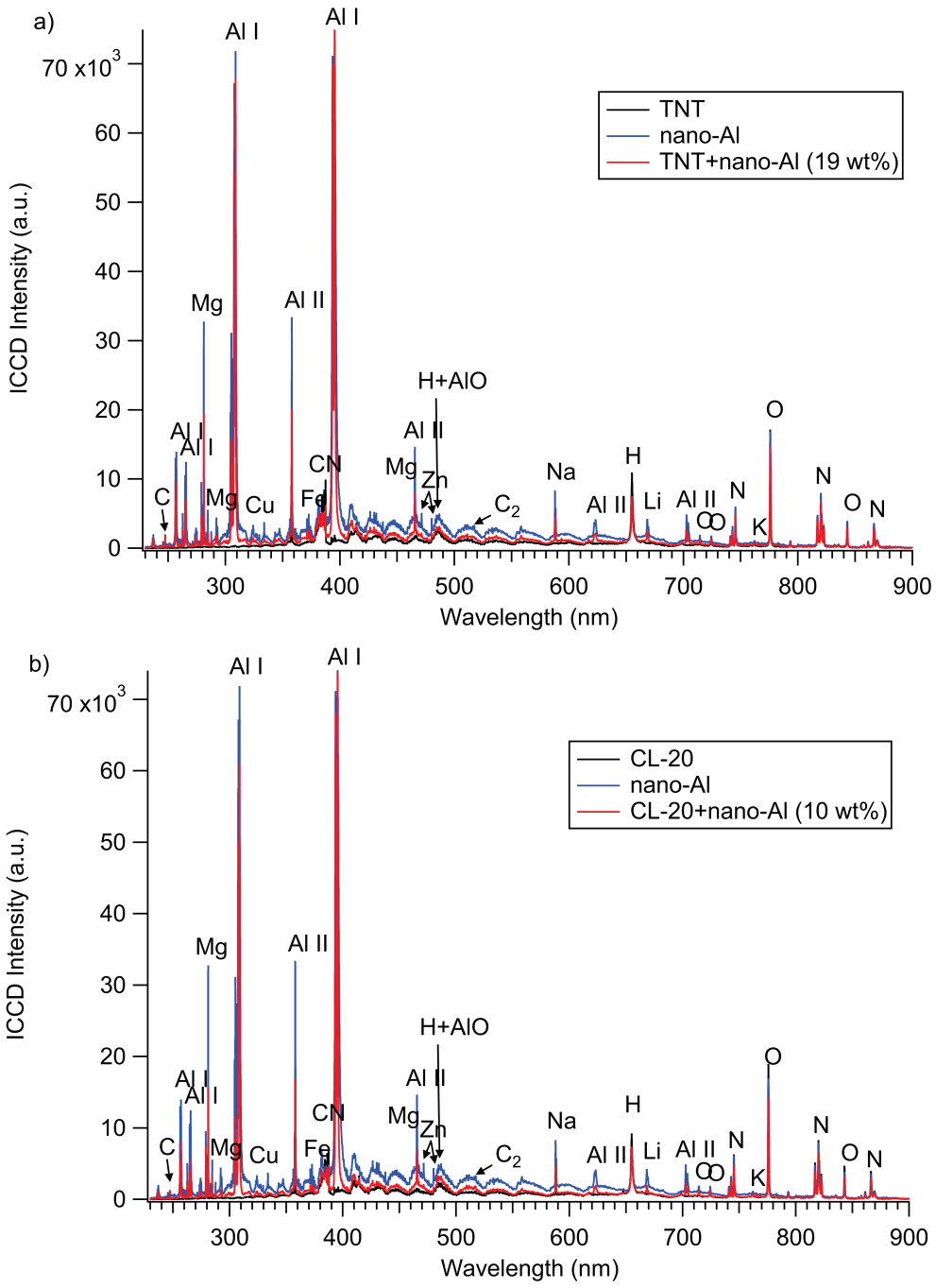

Fig. 9 High-resolution laser-induced plasma emission spectra integrated over 10 μs for the a) TNT and b) CL-20 mixtures with and without nano-Al. Prominent emission features have been labeled.

The relative emission intensities and ratios for the current samples are shown in Fig. 10. The addition of nano-Al tends to decrease the C, CN, H, N, and O emission intensities. The C_2 emission increases with the addition of nano-Al, indicating an oxygen-poor environment preventing the formation of carbon monoxide (CO) and

carbon dioxide (CO_2). The AlO emission is challenging to track because the strongest emission bands are superimposed on the broad H_β line at 486 nm, but the increase in AlO emission with the presence of nano-Al is detectable. Similarly, with the addition of nano-Al, the O/C, H/C, and CN/C ratios decrease, while O/CN and C_2/C increase. We also note that the CL-20 + nano-Al mixture has more AlO emission relative to Al than either TNT + nano-Al or nano-Al, presumably due to the higher oxygen content of CL-20 ($C_6H_6N_{12}O_{12}$) compared to TNT ($C_7H_5N_3O_6$), as discussed in Part II.[2] While some air from the surrounding environment is entrained into the laser-induced plasma and contributes to both the plasma chemistry and emission intensities, Fig. 11 shows the correlation between O and N depends on the sample as well.

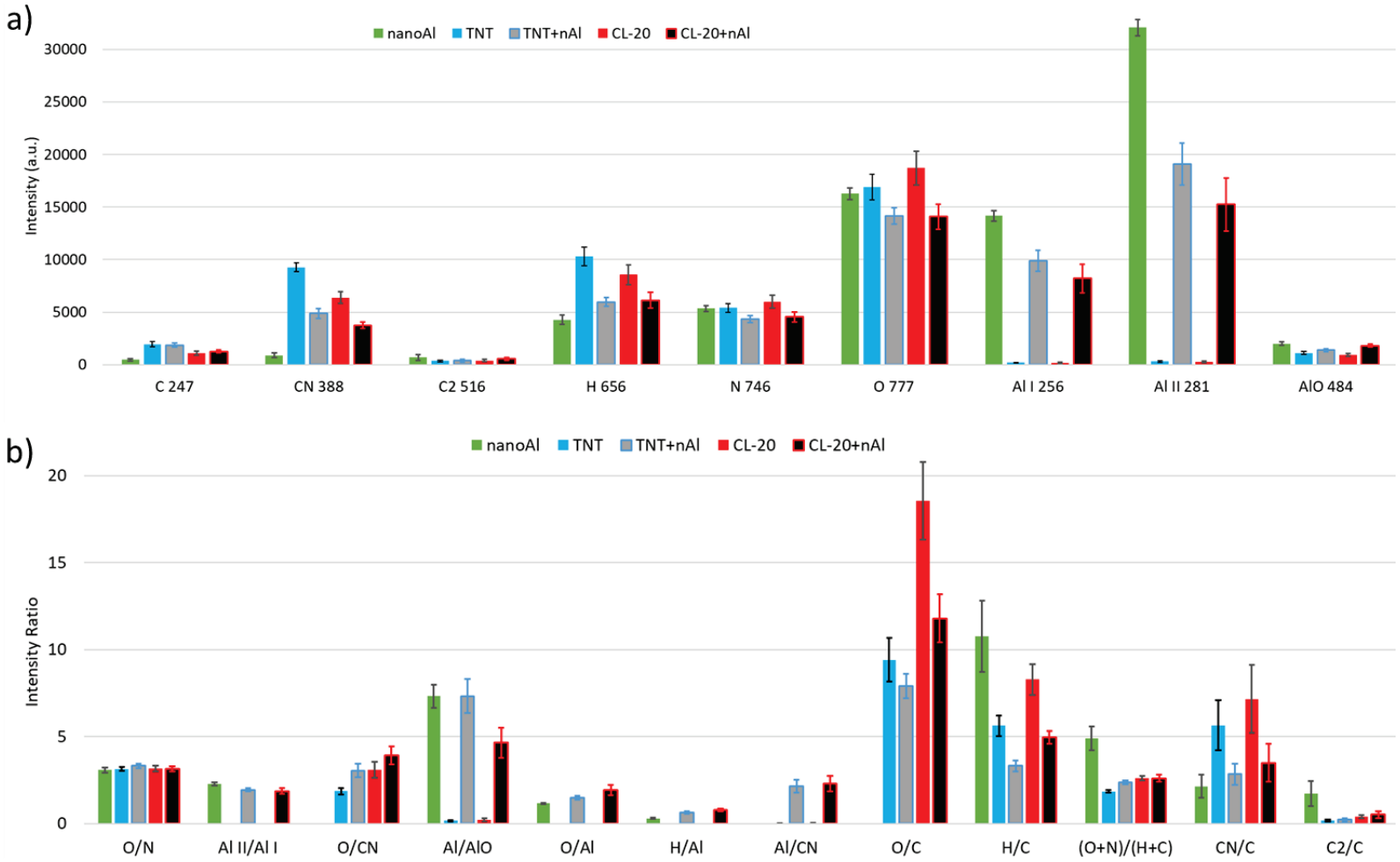

Fig. 10 **a) Background-corrected, maximum plasma emission intensities and b) emission ratios for the nano-Al, TNT, TNT + nano-Al, CL-20, and CL-20 + nano-Al. Error bars are 95% confidence intervals.**

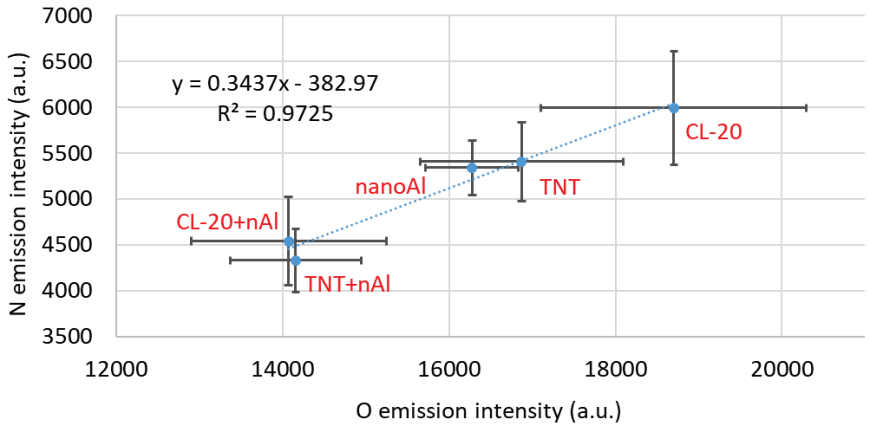

Fig. 11 Correlation between O and N emission intensities in the laser-induced plasma. Error bars are 95% confidence intervals.

3.5.2 Calculated Plasma Temperatures and Electron Densities

Based on the procedure detailed in Part II of this report series,[2] the laser-induced plasma temperatures for each sample (spatially integrated over the entire plasma and temporally integrated over 10 μs) were calculated based on the H_α, H_β, and H_γ emission lines (Fig. 12a). The nano-Al plasma had the highest temperature, and the addition of nano-Al to either TNT or CL-20 also increased the plasma temperature. The oxidation of Al has previously been shown to increase plasma[14,37] and detonation temperatures.[38] A comparison of the electron densities calculated based on the width of the H_α emission line as detailed in Part II[2] shows that although the measurement error is quite large, the electron densities for the samples containing nano-Al are higher than for either pure TNT or pure CL-20 (Fig. 12b). The fact that the characteristic laser-induced shock velocities were lower with the addition of nano-Al while the plasma temperatures and electron densities were higher could potentially be explained by 1) the kinetics of the reactions, that is, the temperature measurements are integrated over 10 μs while the shock wave is influenced by the plasma reactions for a shorter period of time; 2) the plasma may not be in local thermodynamic equilibrium during the spectral gate window (i.e., the calculated H temperatures may not reflect the Al, vibrational, rotational, or ionic plasma temperatures); or 3) other properties such as the kinetic energy of the ejected/reacting material or the formation of product gases not detectable via emission spectroscopy (e.g., CO_2) could more strongly influence the laser-induced shock velocity than the plasma temperature.

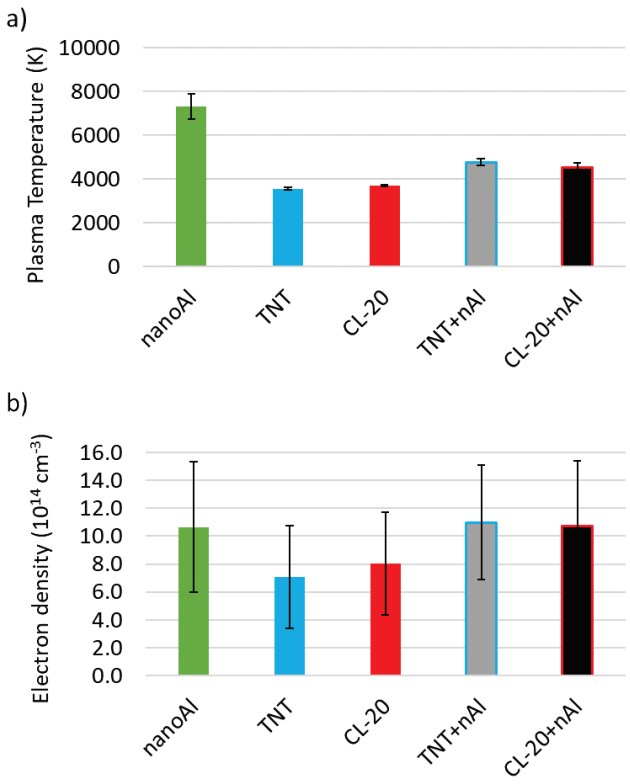

Fig. 12 Calculated a) plasma temperatures and b) electron densities based on H emission lines. Error bars are 95% confidence intervals.

Using the CHEETAH[36] calculations previously discussed, the measured laser-induced plasma temperatures versus the calculated detonation temperatures are shown in Fig. 13. In Part II,[2] we showed that the measured plasma temperatures for the pure explosives were strongly correlated with the calculated detonation temperatures (R^2 = 0.9737). Based on the calculated detonation temperatures, the plasma temperatures for the aluminized explosives are even higher than expected. Together with the lower-than-expected estimated detonation velocities (Fig. 6), this suggests that CHEETAH underestimates the contribution of nano-Al to the detonation chemistry —or that the conditions in the laser-induced plasma make the nano-Al more reactive than it would be under detonation conditions. We note that LASEM estimates of detonation velocities for explosive mixtures with micron-Al agreed well with CHEETAH calculations.[15]

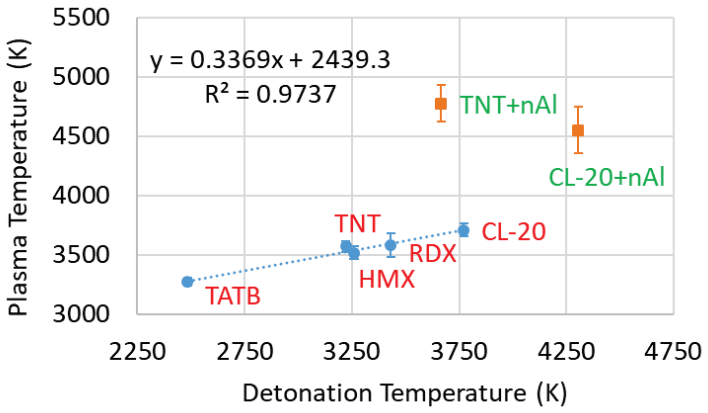

Fig. 13 Correlation between experimentally determined laser-induced plasma temperatures and the calculated detonation temperatures of TNT and CL-20 with and without nano-Al

3.6 Time-Resolved AlO and H Emission

The time-resolved emission signal from the H_α line at 656 nm showed that the PMT signal dropped to the baseline within 15 μs for all samples. Because of the differences in gain settings for the neat explosives and aluminized explosives, the signals were difficult to compare at very early times when plasma continuum emission is also present and the responsivity of the detectors at different gain settings is not known. However, the differences in AlO emission on a longer timescale are readily comparable on the timescale of tens of microseconds, when plasma ignition of ejected particles occurs (Fig. 14). The addition of TNT to nano-Al increases the time to peak AlO emission in this regime from 52 to 73 μs. In contrast, the addition of CL-20 to nano-Al does not significantly affect the time to peak AlO emission. This suggests differences in the explosive mixture chemistry influence the Al oxidation rate on this timescale.

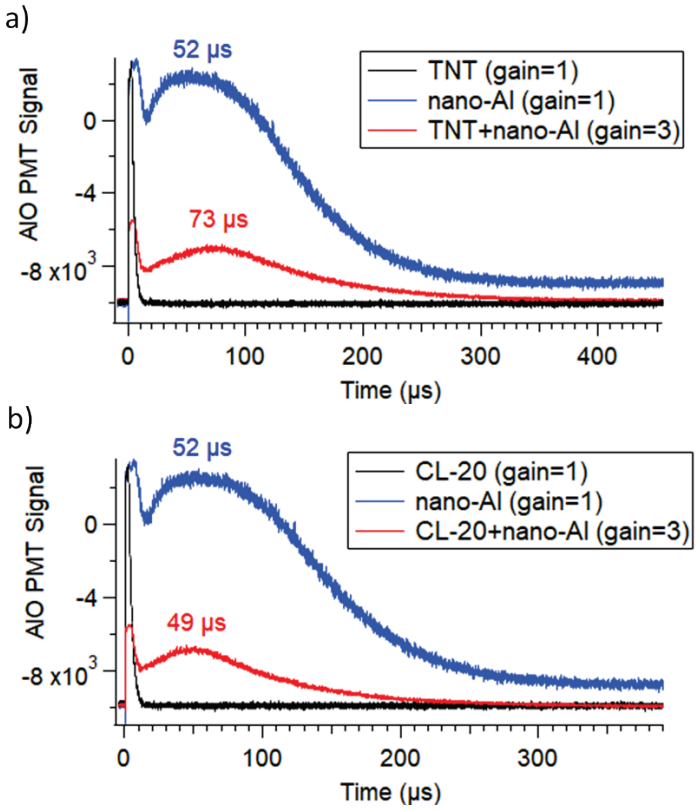

Fig. 14 Time-resolved measurements of the AlO emission line at 486 nm for a) TNT with and without nano-Al and b) CL-20 with and without nano-Al. Neat nano-Al is also shown for comparison.

3.7 Chemistry of Aluminized TNT and CL-20

To investigate the differences in reaction chemistry, the predicted detonation products calculated using CHEETAH[36] were compared for TNT, TNT + 19% Al, CL-20, and CL-20 + 10% Al. For the purposes of the calculations, 100% of the Al was considered active during the detonation chemistry. The detonation products at a) the Chapman–Jouguet (CJ) adiabat, b) at room temperature and pressure, or c) in 99% air are shown in Fig. 15. According to the thermochemical code, the addition of Al increases the CO, CH_4, NH_3, and H_2 for both TNT and CL-20. The N_2 decreases slightly with the addition of Al, while the CO_2 and H_2O drop significantly for both explosives. This is because the Al preferentially scavenges the available O, such that the C cannot be fully oxidized.

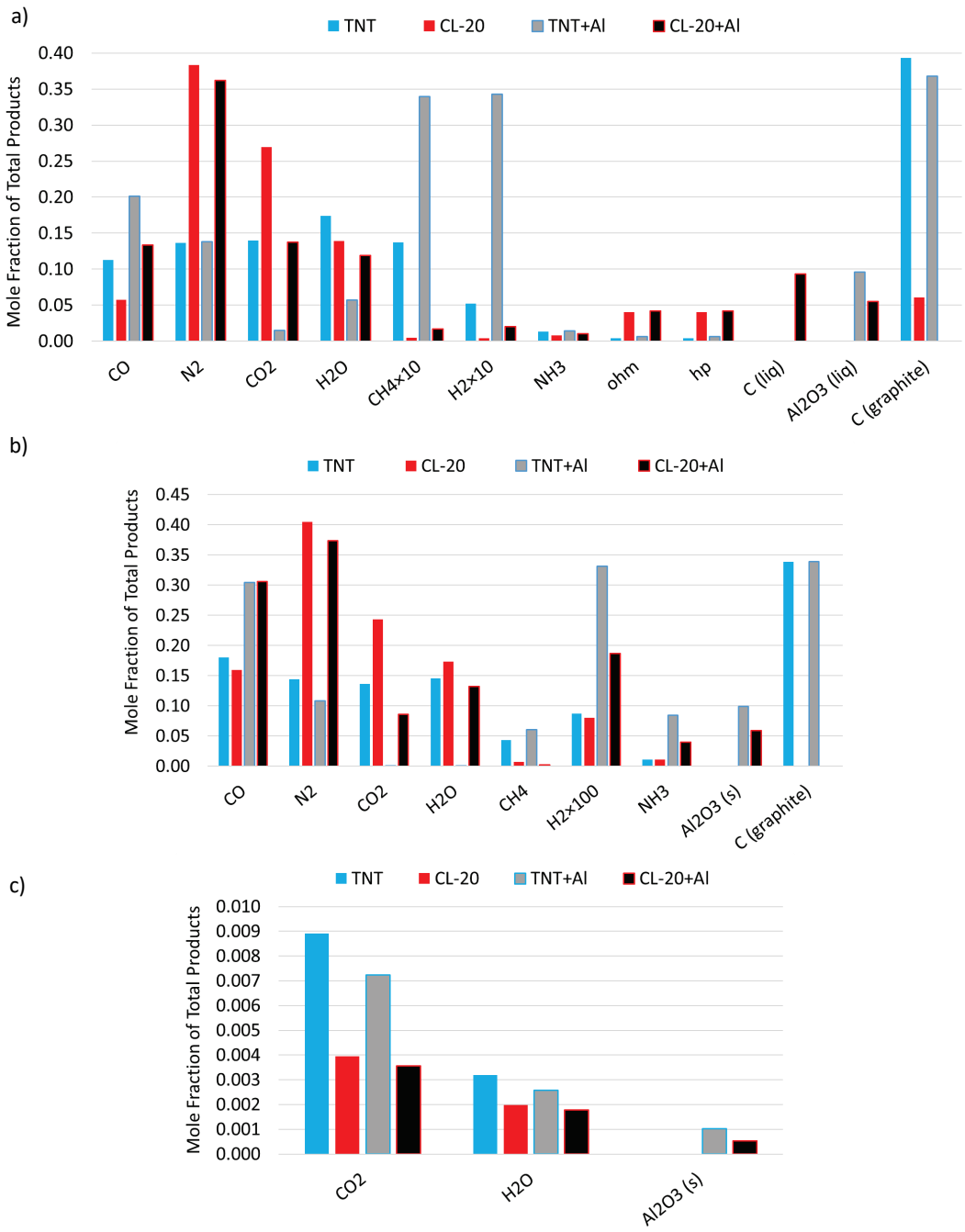

Fig. 15 Predicted detonation products for TNT and CL-20 with and without active Al (19% or 10%, respectively) at a) the CJ adiabat, b) room temperature and pressure, or c) in 99% air, as calculated with CHEETAH.[36] Neither N_2 (~0.79) or O_2 (~0.21) are included in the products under air since they are similar for all samples.

3.8 NIR Emission Spectroscopy

Sequential NIR emission spectra were acquired for the samples and are shown in Fig. 16 (the spectra for neat nano-Al were shown in Part I).[1] The spectrometer was saturated for both the TNT and TNT + nano-Al during the peak combustion reactions. Example spectra from the series are shown in Fig. 17. While the addition of nano-Al to TNT does not significantly affect the NIR emission spectra (Fig. 17a), the CL-20 spectra are strongly influenced by the presence of nano-Al (Fig. 17b). The tentative feature assignments were described in detail in Part II.[2] As shown in Fig. 15a, while neat CL-20 has very little CH_4, the CH_4 concentration increases for CL-20 + 10% Al at high temperatures. This difference in chemistry could explain the change in the NIR emission spectra with the addition of nano-Al, which is then similar to that of the TNT spectra (with or without nano-Al).

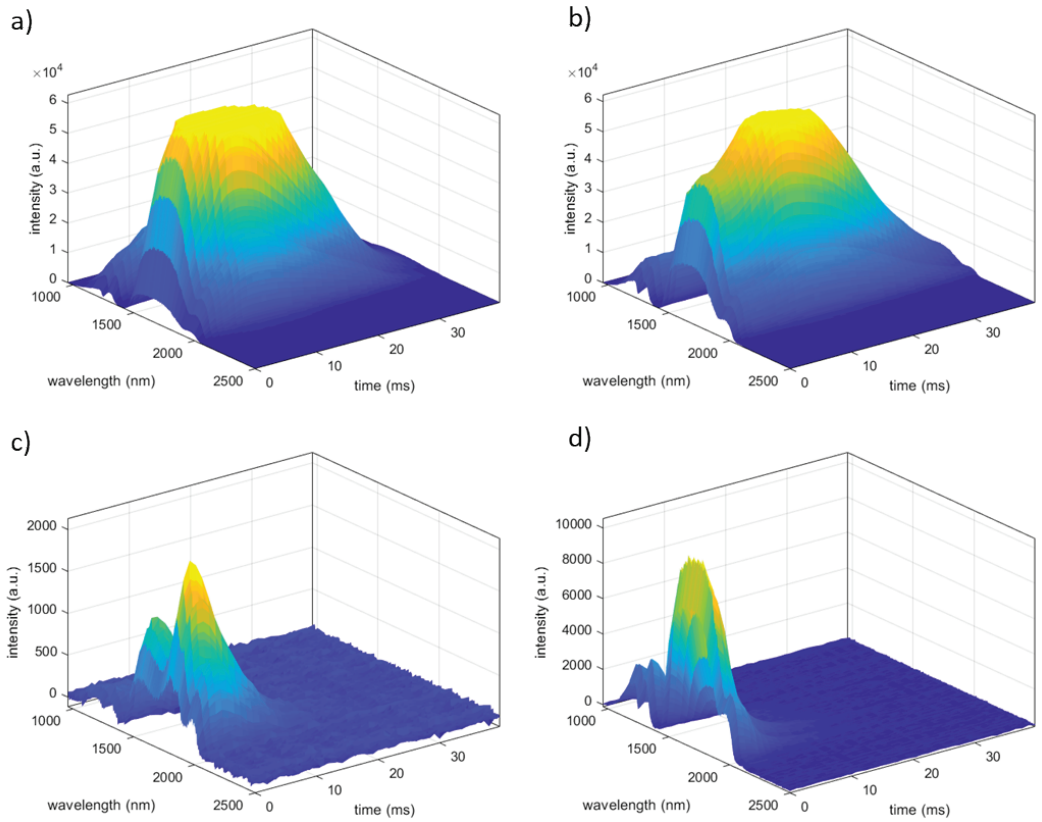

Fig. 16 Sequential NIR emission spectra acquired following pulsed laser excitation of the a) TNT, b) TNT + 19% nano-Al, c) CL-20, and d) CL-20 + 10% nano-Al (representative series for each sample shown)

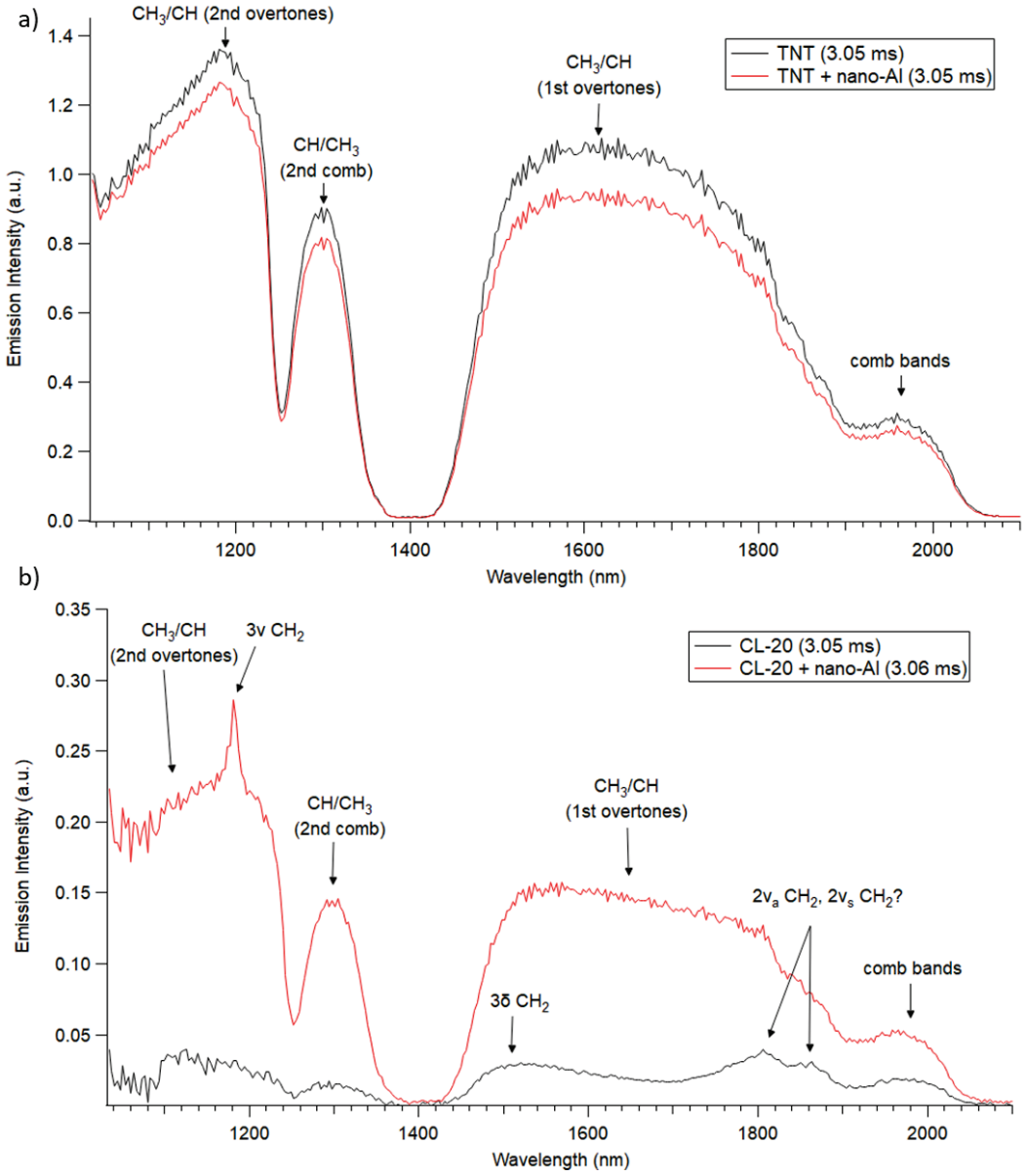

Fig. 17 Selected intensity-corrected spectra from the sequentially obtained series of NIR emission spectra for a) TNT and TNT + 19% nano-Al and b) CL-20 + 10% nano-Al

3.9 Visible Emission Spectroscopy

The combustion emission spectra (gated to avoid laser-induced plasma emission) are shown in Fig. 18. In contrast to TNT + 20% micron-Al, where the combustion reactions increase in intensity compared to neat TNT,[15] the addition of nano-Al decreases the combustion intensity of TNT on the millisecond timescale. This is due to the faster reactions of nano-Al compared to micron-Al; on the millisecond timescale, most of the nano-Al has already oxidized. Some larger particles continue to combust on this timescale, however, as demonstrated by the appearance of AlO

emission features. The appearance of the atomic O and N emission features, which have high excited state energy levels, in the combustion spectra of aluminized explosives suggest that the combustion temperatures increase with the addition of nano-Al. Since CL-20 reacts much faster than TNT, there may be less available O for the nano-Al to react with at earlier times in the CL-20 + nano-Al mixture—resulting in an increase in combustion at later times as the remaining nano-Al reacts with air entrained in the reaction region (Fig. 18b).

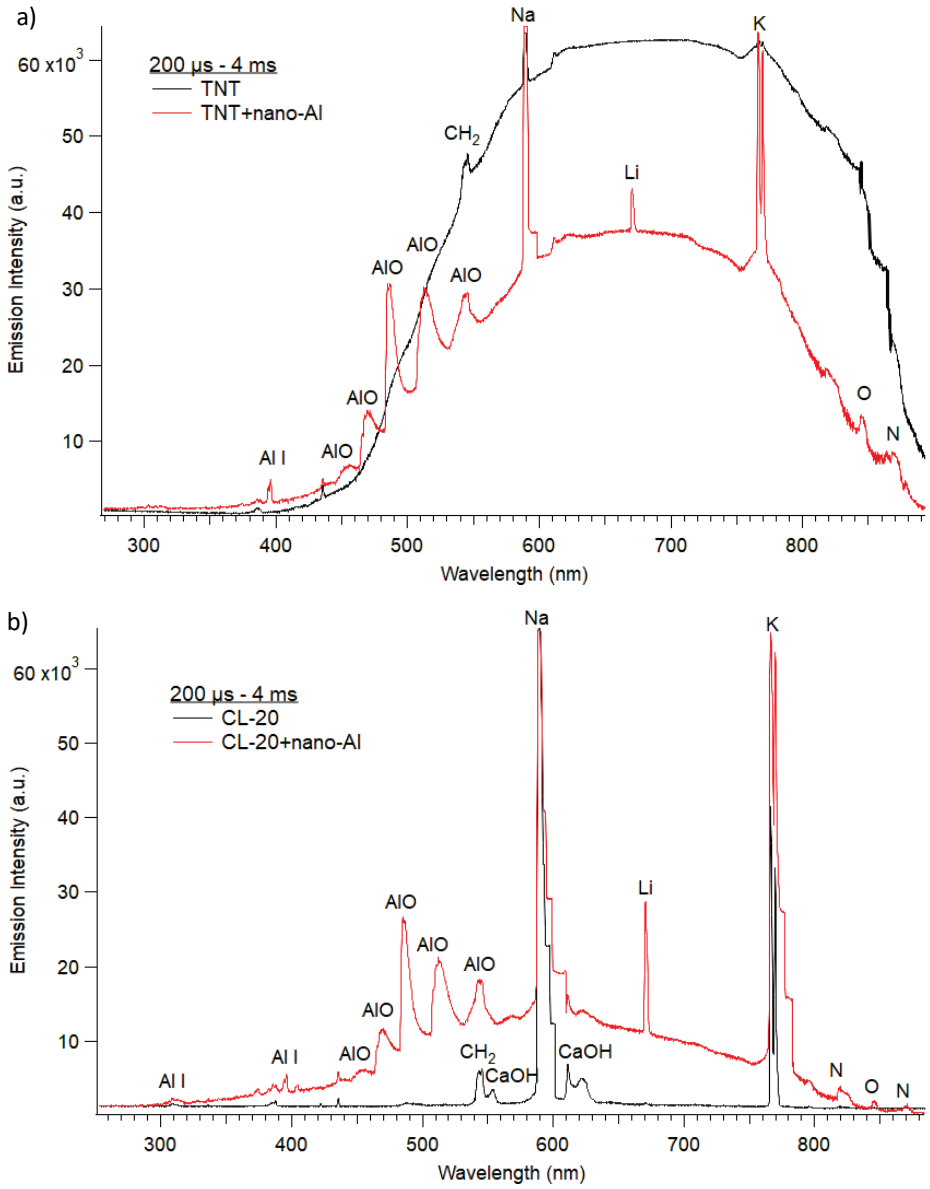

Fig. 18 Combustion emission spectra for a) TNT and TNT + 19% nano-Al and b) CL-20 and CL-20 + 10% nano-Al, integrated from 200 µs to 4 ms after the pulsed laser excitation. Broadband gray-body emission and molecular emission dominate the spectra in this regime, in addition to strong alkali metal emission.

The sequentially obtained visible emission spectra are shown in Fig. 19. Although the spectra were acquired out to around 100 ms, they have been truncated for the figure since no emission was detected at later times. The clear transition between atomic/ionic emission from the laser-induced plasma to primarily gray-body/molecular combustion emission is evident in the spectra. Selected spectra from the sequential series in Fig. 19 are shown in Fig. 20, along with spectral assignments to illustrate the differences in the time regimes. Adding nano-Al decreases the CN and H emission intensities from TNT (but not CL-20).

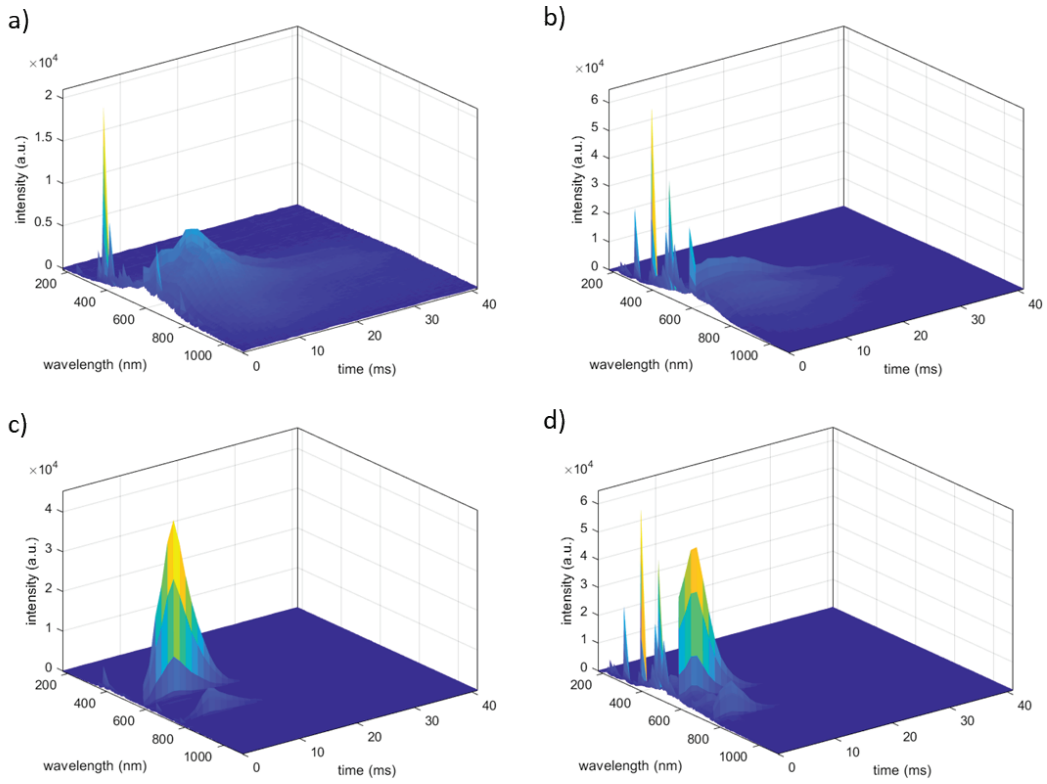

Fig. 19 Sequential visible emission spectra acquired following pulsed laser excitation of the a) TNT, b) TNT + 19% nano-Al, c) CL-20, and d) CL-20 + 10% nano-Al (representative series for each sample shown)

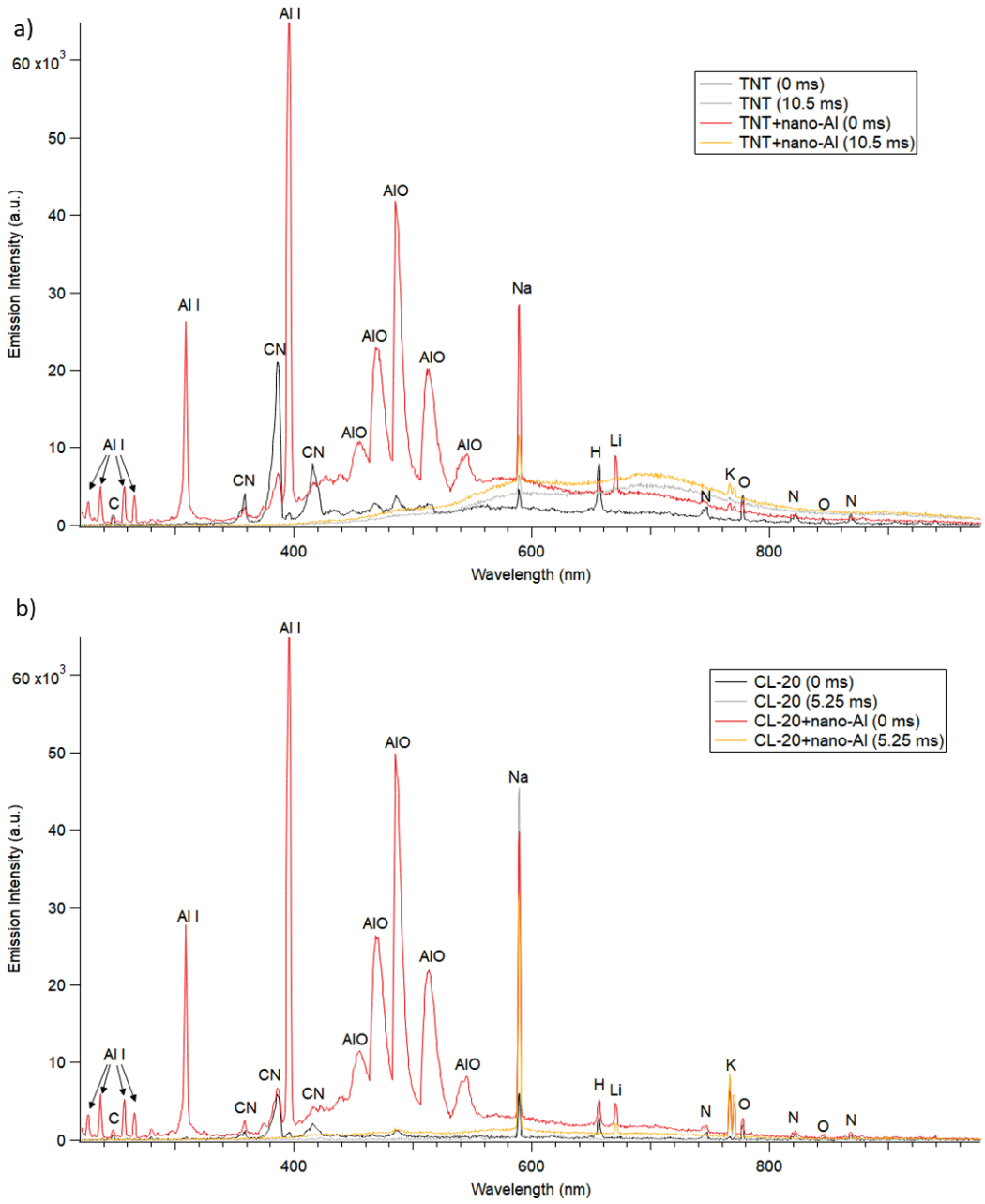

Fig. 20 Selected spectra from the sequentially obtained series of visible emission spectra for a) TNT and TNT + 19% nano-Al and b) CL-20 and CL-20 + 10% nano-Al

As shown in Fig. 21a, most of the nano-Al is oxidized in the first millisecond of the laser-induced chemical reactions. A secondary peak in AlO emission occurs around 2 ms for the CL-20 + nano-Al sample. Overall, the spectra at later times are relatively weak due to dynamic range limitations for the spectrometer. The peak in O emission for CL-20 + nano-Al coincides with the peak in AlO emission (Fig. 21b). Interestingly, even larger peak O intensities occur around 8 ms for the TNT and TNT + nano-Al samples—without the accompanying AlO emission. This

suggests the O peak near 8 ms is primarily due to the combustion of TNT particles as they are ejected into the air heated by the laser-induced plasma and passage of the laser-induced shock wave.[39]

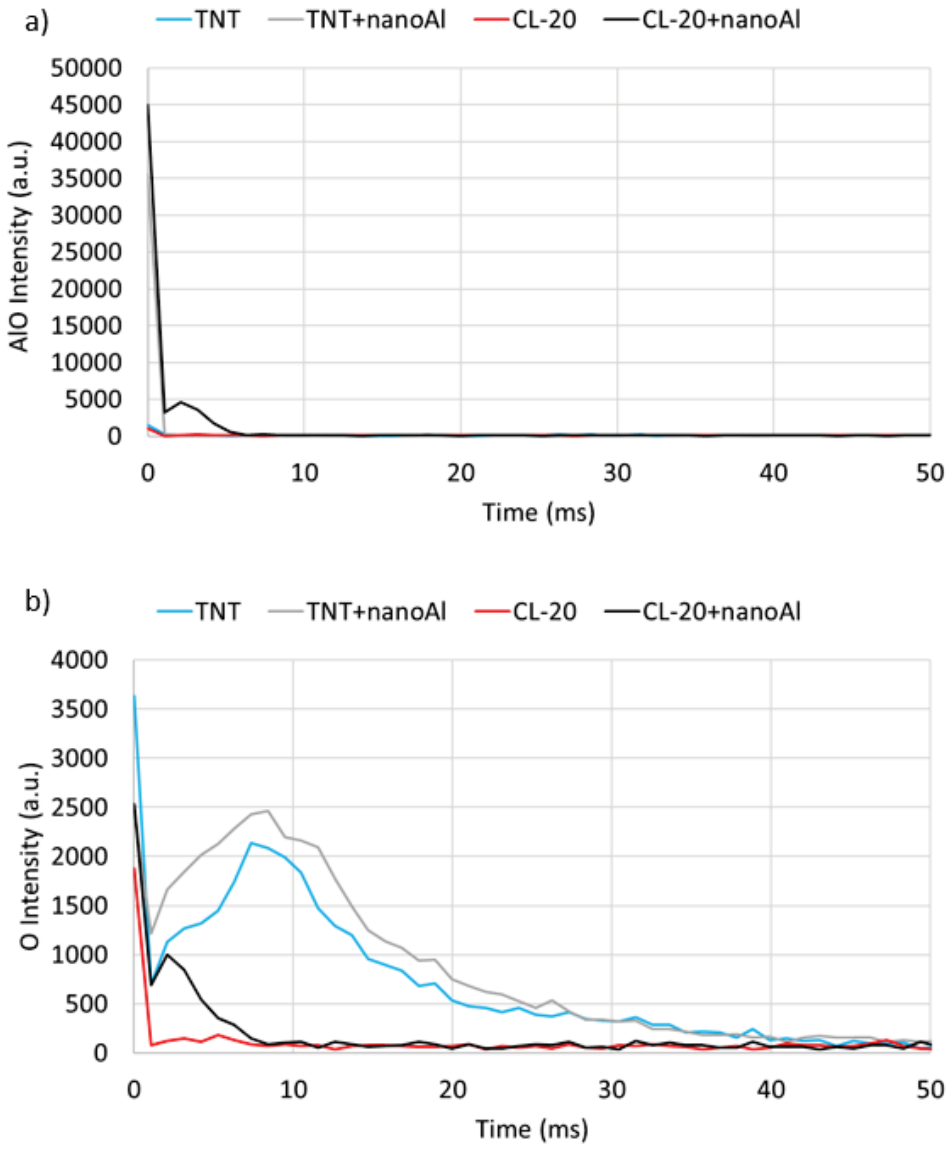

Fig. 21 Time-resolved, background-corrected peak a) AlO (486-nm) and b) O (777-nm) emission intensities from the spectra in Fig. 19

3.10 Integrated IR Emission

As shown in Fig. 22 (and discussed in Section 3.9), the addition of nano-Al decreases the intensity of the TNT combustion. In contrast, the IR emission from the combustion of CL-20 is significantly increased in intensity by the presence of

nano-Al. For TNT, the time to peak combustion is decreased with the addition of nano-Al while it slightly increases the time to peak combustion of CL-20.

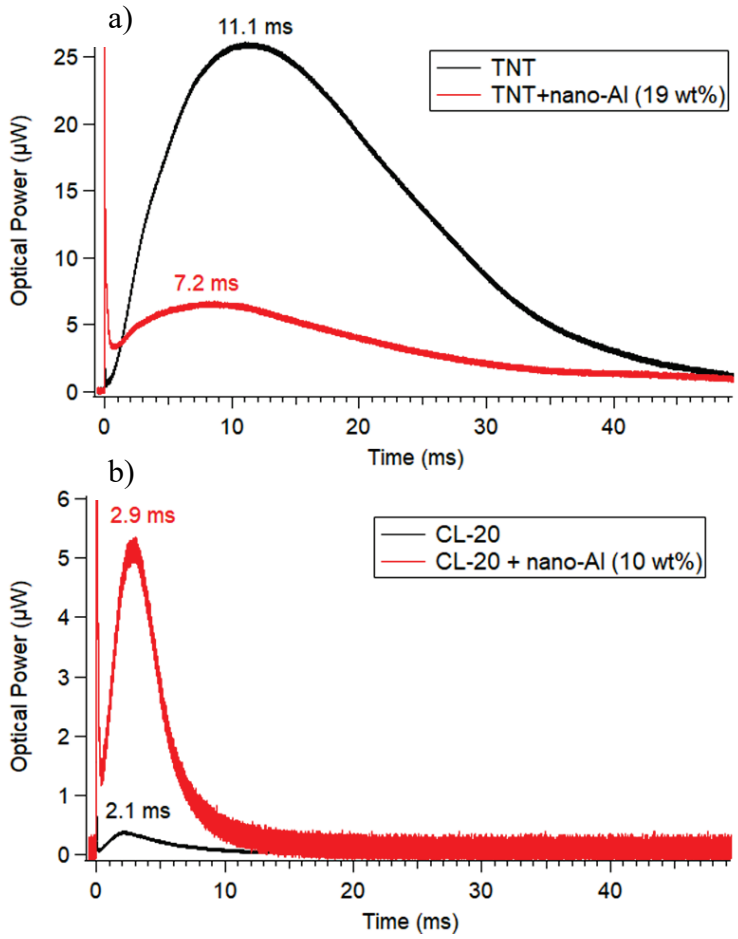

Fig. 22 Time-resolved, spatially and spectrally integrated IR emission following laser excitation of a) TNT and TNT + 19% nano-Al and b) CL-20 and CL-20 + 10% nano-Al. The first sharp spike in emission is due to the laser-induced plasma, followed by the combustion emission on the millisecond timescale.

4. Conclusion

For both TNT and CL-20, the addition of either 19% or 10% by weight nano-Al, respectively, resulted in:

- Increased plasma emission, which obscured the laser-induced shock wave for longer (i.e., more camera frames);
- Changes in the relative laser-induced shock wave positions on the microsecond timescale (compared to the neat explosives), indicating complex chemistry;

- Significant reduction in the characteristic laser-induced shock wave velocities, the chemical energy behind the shock waves, and the temperatures of the surrounding air;
- Decreased plasma emission from C, CN, H, N, and O;
- Increased plasma emission from C_2 (due to Al scavenging O from the explosive, reducing the formation of CO_2);
- Increased plasma temperatures and electron densities (based on the H emission features integrated over 10 μs);
- Measured plasma temperatures are higher than expected based on the calculated detonation temperatures of the aluminized explosives, suggesting either CHEETAH[36] underestimates the contribution of nano-Al to the detonation chemistry or that the conditions in the laser-induced plasma make the nano-Al more reactive than it would be under detonation conditions; and
- Decreased CO_2 and H_2O production (predicted by CHEETAH).[36]

The addition of 19% nano-Al to TNT also demonstrated that:

- The effect of nano-Al on the estimated detonation velocity of TNT is more pronounced than with either micron-Al or a strongly agglomerated Al nanoparticle sample;
- The addition of nano-Al to TNT increases the time to peak AlO emission on the intermediate timescale (i.e., plasma ignited combustion) from 52 to 73 μs;
- The NIR emission spectra were not significantly influenced by the addition of nano-Al;
- The combustion intensity on the millisecond timescale decreased with the addition of nano-Al, although the presence of strong O and N emission suggests higher combustion temperatures;
- During combustion, the CN and H emission intensities decreased with the addition of nano-Al to TNT;
- The average time to peak combustion on the millisecond timescale decrease from 11.1 to 7.2 ms; and
- Sequential emission spectra show that most of the Al oxidation occurs within 1 ms, followed by a peak in O emission near 8 ms that coincides with combustion of TNT particles.

In contrast to TNT, the addition of 10% nano-Al to Cl-20 resulted in:

- An estimated detonation velocity that is significantly lower than that predicted by the thermochemical code CHEETAH[36], assuming 100% of the Al is active;
- Increased microsecond-timescale emission from AlO compared to TNT + nano-Al or neat nano-Al (presumably due to the higher O content in CL-20);
- Similar times to peak AlO emission on the intermediate timescale for both CL-20 and CL-20 + nano-Al (~50 μs);
- Significant changes in the NIR emission spectra were observed with the addition of nano-Al, suggesting differences in the reaction products (e.g., an increase in CH_4, as predicted by CHEETAH[36]);
- During combustion, the CN and H emission intensities did not change with the addition of nano-Al to CL-20;
- Increased combustion intensities on the millisecond timescale with a slight increase in the average time to peak combustion from 2.1 to 2.9 ms; and
- Substantial Al oxidation occurs within 1 ms, followed by an additional AlO emission peak near 2 ms that coincides with a peak in O intensity.

5. References

1. Gottfried JL. Higher time-resolution LASEM, part I: influence of aluminum morphology on laser-induced shock waves and chemistry. Aberdeen Proving Ground (MD): CCDC Army Research Laboratory (US); 2020 Aug. Report No.: ARL-TR-9020.

2. Gottfried JL, Barnes BC. Higher time-resolution LASEM, part II: influence of plasma chemistry on the laser-induced shock waves of explosives. Aberdeen Proving Ground (MD): CCDC Army Research Laboratory (US); 2020 Aug. Report No.: ARL-TR-9026.

3. Gottfried JL. Influence of exothermic chemical reactions on laser-induced shock waves. Phys Chem Chem Phys. 2014;16:21452–21466.

4. Vadhe PP, Pawar RB, Sinha RK, Asthana SN, Rao AS. Cast aluminized explosives. Combust Explos. 2008;44(4):461–477.

5. Yen NH, Wang LY. Reactive metals in explosives. Propellants Explos Pyrotech. 2012;37(2):143–155.

6. Zygmunt A, Gańczyk-Specjalska K, Kasztankiewicz A, Cieślak K, Gołofit T. Application and properties of aluminum in primary and secondary explosives. J Element. 2017;22(2):747–759.

7. Kasztankiewicz A, Gańczyk-Specjalska K, Zygmunt A, Cieślak K, Zakoscielny B, Golofit T. Application and properties of aluminum in rocket propellants and pyrotechnics. J Elem. 2018;23(1):321–331.

8. Comet M, Martin C, Schnell F, Spitzer D. Nanothermites: a short review. Factsheet for experimenters, present and future challenges. Propellants Explos Pyrotech. 2019;44(1):18–36.

9. Thiruvengadathan R. Nano-energetic materials. In: Bhattacharya S, Agarwal AK, Rajagopalan T, Patel VK, editors. Singapore: Springer Nature Singapore Pte Ltd.; 2019. Chapter 2, Aluminum-based nano-energetic materials: state of the art and future perspectives. p. 9–35.

10. Dreizin EL. Metal-based reactive nanomaterials. Prog Energy Combust Sci. 2009;35(2):141–167.

11. Yetter RA, Risha GA, Son SF. Metal particle combustion and nanotechnology. Proc Combust Inst. 2009;32(2):1819–1838.

12. Sundaram DS, Yang V, Zarko VE. Combustion of nano aluminum particles (review). Combust Explos Shock Waves. 2015;51(2):173–196.

13. Dreizin EL, Schoenitz M. Mechanochemically prepared reactive and energetic materials: a review. J Mater Sci. 2017;52(20):11789–11809.

14. Gottfried JL. Laser-induced plasma chemistry of the explosive RDX with various metallic nanoparticles. Appl Opt. 2012;51(7):B13–B21.

15. Gottfried JL, Bukowski EJ. Laser-shocked energetic materials with metal additives: evaluation of chemistry and detonation performance. Appl Opt. 2017;56(3):B47–B57.

16. Gottfried JL, Smith DK, Wu C-C, Pantoya ML. Improving the explosive performance of aluminum nanoparticles with aluminum iodate hexahydrate (AIH). Sci Rep. 2018;8:8036.

17. Miller KK, Gottfried JL, Walck SD, Pantoya ML, Wu C-C. Plasma surface treatment of aluminum nanoparticles for energetic material applications. Combust Flame. 2019;206:211–213.

18. Jiang Y, Deng S, Hong S, Zhao J, Huang S, Wu C-C, Gottfried JL, Nomura K-i, Li Y, Tiwari SC, et al. Energetic performance of optically activated aluminum/graphene oxide composites. ACS Nano. 2018;12:11366–11375.

19. Gottfried J, Wu C, Zheng X. Measuring the fast and slow energy release of laser-excited aluminum/graphene oxide composites. NATO Specialist Meeting on Graphene Technologies and Applications for Defense; 2019; Trondheim, Norway.

20. Wainwright ER, Dean SW, Lakshman SV, Weihs TP, Gottfried JL. Evaluating compositional effects on the laser-induced combustion and shock velocities of Al/Zr-based composite fuels. Combust Flame. 2019;213:357–368.

21. Gottfried JL, Dean SW, Wu C-C, Frank J, De Lucia C. Optimizing the performance of aluminized explosives: laser-based measurements of energy release and spectroscopic diagnostics. Aberdeen Proving Ground (MD): CCDC Army Research Laboratory (US); 2020 Apr. Report No.: ARL-TR-8934.

22. Mao X, Jiang L, Zhu C, Wang X. Effects of aluminum powder on ignition performance of RDX, HMX, and CL-20 explosives. Adv Mater Sci Eng. 2018;5913216.

23. Liu D, Chen L, Wang C, Wu J. Aluminum acceleration and reaction characteristics for aluminized CL-20-based mixed explosives. Propellants Explos Pyrotech. 2018;43(6):543–551.

24. Gottfried JL. Laboratory-scale method for estimating explosive performance from laser-induced shock waves. Propellants Explos Pyrotech. 2015;40(5):674–681.

25. Baudin G, Lefrançois A, Bergues D, Bigot J, Champion Y. Combustion of nanophase aluminum in the detonation products of nitromethane. In: Short J, editor. Proceedings of the 11th International Detonation Symposium; 1998 Aug 31–Sep 4; Snowmass Village, CO. p. 989–997.

26. Miller PJ, Bedford CD, Davis JJ. Effect of metal particle size on the detonation performance of various metallized explosives. In: Short J, editor. Proceedings of the 11th International Detonation Symposium; 1998 Aug 31–Sep 4; Snowmass Village, CO. p. 214–220.

27. Shevchenko AA, Dolgoborodov AY, Kirilenko VG, Brazhnikov MA. Detonation velocity of mechanically activated mixtures of ammonium perchlorate and aluminum. Combust Explos Shock Waves. 2017;53(4):461–470.

28. Price D, Clairmont AR, Erkman JO. Explosive behavior of aluminized ammonium perchlorate. Combust Flame. 1973;20(3):389–400.

29. Tao WC, Tarver CM, Kury JW, Lee CG, Ornellas DL. Understanding composite explosive energetics: 4. Reactive flow modeling of aluminum reaction kinetics in PETN and TNT using normalized product equation of state. Proceedings of the 10th International Detonation Symposium; 1993 July 12–16; Boston, MA; ONR 33395-12. p. 628–636.

30. Cliff MD, Dexter RM, Watt DS. The effect of ultrafine, electroexploded aluminum (alex) on detonation velocity and pressure. Melbourne (Australia): DSTO Aeronautical and Maritime Research Laboratory; 2000. Report No.: DSTO-TR-0999.

31. Lefrançois A, Gallic CL. Expertise of nanometric aluminum powder on the detonation efficiency of explosives. 32nd International Annual Conference of ICT; 2001 July 3–6; Karlsruhe, Germany. p. 36–1.

32. Brousseau P, Cliff MD. The effect of ultrafine aluminum powder on the detonation properties of various explosives. 32nd International Annual Conference of ICT; 2001 July 3–6; Karlsruhe, Germany. p. 37–1.

33. Brousseau P, Anderson CJ. Nanometric aluminum in explosives. Propellants Explos Pyrotech. 2002;27(5):300–306.

34. Dorsett H, Cliff MD. Detonation front curvature measurements and aquarium tests of tritonal variants. Defence Science and Technology Organisation, Edinburgh, South Australia; 2003. Report No.: DSTO-TR-1411.

35. Zhou ZQ, Chen JG, Yuan HY, Nie JX. Effects of aluminum particle size on the detonation pressure of TNT/Al. Propellants Explos Pyrotech. 2017;42(12)1401–1409.

36. Bastea S, Fried LE, Glaesemann KR, Howard WM, Kuo I-FW, Souers PC, Vitello PA. CHEETAH 8.0. Livermore (CA): Energetic Materials Center, Lawrence Livermore National Laboratory.

37. Wainwright ER, Dean SW, De Lucia Jr FC, Weihs TP, Gottfried JL. Effect of sample morphology on the spectral and spatiotemporal characteristics of laser-induced plasmas from aluminum. Appl Phys A. 2020;126.

38. Gogulya MF, Makhov MN, Dolgoborodov AY, Brazhnikov MA, Arkhipov VI, Shchetinin VG. Mechanical sensitivity and detonation parameters of aluminized explosives. Combust Explos. 2004;40(4):445–457.

39. Collins ES, Gottfried JL. Laser-induced deflagration for the characterization of energetic materials. Propellants Explos Pyrotech. 2017;42(6):592–602.

List of Symbols, Abbreviations, and Acronyms

Al	aluminum
AlO	aluminum monoxide
ARL	Army Research Laboratory
C	carbon
C_2	diatomic carbon
CCDC	US Army Combat Capabilities Development Command
CH_4	methane
CJ	Chapman–Jouguet
CL-20	hexanitrohexaazaisowurtzitane
CN	cyano radical
CO	carbon monoxide
CO_2	carbon dioxide
Cu	copper
Fe	iron
fps	frames per second
H	hydrogen
H_2O	water
HMX	cyclotetramethylene tetranitramine
ICCD	intensified charge-coupled detector
IR	infrared
K	potassium
LASEM	laser-induced air shock from energetic materials
Li	lithium
Mg	magnesium
micron-Al	micrometer-sized Al
N	nitrogen
Na	sodium
N/A	not applicable
nano-Al	Al nanoparticles

NH	imidogen
NIR	near-infrared
O	oxygen
PMT	photomultiplier tube
RDX	cyclotrimethylene trinitramine
TATB	triaminotrinitrobenzene
TNT	trinitrotoluene
Zn	zinc
Zr	zirconium

1 (PDF) DEFENSE TECHNICAL INFORMATION CTR DTIC OCA

1 (PDF) CCDC ARL FCDD RLD CL TECH LIB

1 (PDF) CCDC ARL FCDD RLW LB J GOTTFRIED